Flood estimation for ungauged catchments in the Philippines

<u>Integrating historical archives and geospatial data to revise</u> flood estimation equations for Philippine rivers

Trevor B. Hoey¹, Pamela L.M. Tolentino^{2,3}, Esmael Guardian³, John Edward G. Perez^{3,4}, Richard D. Williams², Richard Boothroyd⁵, Carlos Primo C David³ and Enrico Paringit^{6,7}

- ¹ Department of Civil and Environmental Engineering, Brunel University London, London, UB8 3PH, United Kingdom
- ² School of Geographical and Earth Sciences, University of Glasgow, Glasgow, G12 8QQ, United Kingdom
- ³ National Institute of Geological Sciences, University of the Philippines Diliman, Philippines
- ⁴University of Vienna, Vienna, Austria
 - ⁵ Department of Geography and Planning, University of Liverpool, Liverpool, L69 7ZT, United Kingdom
 - ⁶ Department of Geodetic Engineering, University of the Philippines Diliman, Philippines
 - ⁷ Department of Science and Technology Philippine Council for Industry, Energy and Emerging Technology Research and Development
- 15 Correspondence to: Pamela Louise M. Tolentino (Pammie.Tolentino@glasgow.ac.uk)

1 Abstract

20

25

30

35

40

45

Flood magnitude and frequency estimation are essential for the design of structural and nature-based flood risk management interventions and water resources planning. However, the global geography of hydrological observations is uneven; in many regions, such as the Philippines, data are spatially and/or temporarily sparse, limiting the choice of statistical methods for flood estimation. We evaluate the potential of pooling short historical data series to estimate flood magnitudes at national scale for ungauged catchment flood estimation. Daily mean river discharge data were collected from publications covering 842 sites, with data spanning from 1908 to 20181991. Of these, 513 466 candidate sites met criteria to estimate a reliable annual maximum flood. Using the index flood approach, a range of controls were assessed at national and regional scales using land cover and rainfall datasets, and GIS-derived catchment characteristics. Multivariate analysis for predictive equations for 2to 100-year recurrence interval floods based on catchment area only have $R^2 \le 0.59$. Additionally, adding a rainfall variable, the median annual maximum 1-day rainfall, increases \mathbb{R}^2 to between 0.56 for Q_{100} and 0.66 for Q_2 . Very few other variables were significant when added to multiple regression equations and Relatively low R² values are typical of studies from tropical regions. Although the Philippines exhibits regional climate variability, there is limited spatial structure in predictive equation residuals and region-specific predictive equations do not perform significantly better than national equations. Relatively low R² values are typical of studies from tropical regions. The predictive equations are suitable for use as design equations in ungauged catchments for the Philippines but uncertainties must be assessed. Our approach demonstrates how combining individually short historical records, after careful screening and exclusion of erroneous data, generates large data sets that can produce consistent results. Extension of continuous flood records is required to reduce uncertainties but national-scale consistency suggests that extrapolation from a small number of carefully selected catchments could provide nationally reliable predictive equations with reduced uncertainties.

2 Introduction and rationale

The impact of river flooding across Southeast Asia is severe on a global scale, whether measured in terms of inundated area, the number of people affected or fatalities (Ziegler et al., 2020). Understanding the hazard and designing mitigation or adaptation strategies relies on estimating flood magnitude and frequency, which is achieved through empirical analyses of available data and, for forecasting, the results of climate and hydrological models. The resulting equations to estimate flows of specified recurrence are used for a wide range of purposes including insurance loss estimation (Lyubchich et al., 2018), aquatic biodiversity assessment (Parasiewicz et al., 2019), engineering design and water resource planning.

55

60

65

70

75

80

85

90

95

A wide range of statistical methods have been applied to flood frequency estimation (see Asquith et al., 2017 for a recent listing). The index flood approach uses the median or mean annual maximum flood, or equivalently a flood of specified recurrence interval, and relates this to catchment properties to develop regional predictive equations (eg Dalrymple, 1960; Kjeldsen and Jones, 2006; Stedinger and Lu, 1995). In data-rich settings, such approaches can be complex, as illustrated by the United Kingdom (UK) Flood Estimation Handbook (FEH). Kjeldsen et al. (2008; Table 4.1) show how successive iterations of predictive equations for the UK have added variables and statistical complexity. However, catchment area and annual precipitation remain the most significant predictors even in this case (Meigh et al., 1997). Although the index flood method is reliable and can yield high R² values, adding non-linear effects and spatially-dependent interactions have been proposed as potential sources of further improvement (Muhammad and Lu, 2020).

In many countries, and regions river flow data may be sparse in space and/or time (Mamun et al., 2011), limiting the choice of statistical methods for flood frequency estimation and strongly influencing the magnitude of associated uncertainties. The lengths of records that are available impacts on the analytical results (Fischer and Schumann, 2022), and uncertainty increases with short data series. This uncertainty can be reduced by extending data series through use of historical or proxy information (Macdonald et al., 2014; Merz and Blöschl, 2008; Reinders and Muñoz, 2021; Ziegler et al., 2020), by cross-validation against hydrological modelling predictions (Haberlandt and Radtke, 2014), or by pooling information from many sites (Kjeldsen, 2015; Griffiths et al., 2020).

For the Philippines, which exemplifies some of the challenges of using sparse hydrological data, some national-scale analyses of flood magnitude and frequency have been undertaken. Meigh (1995) analysed data, mostly from up to 1980, from 333 sites collected by the BRS (Bureau of Research and Standards). Growth curves and prediction equations for flood magnitude were presented for different hydrological regions and catchment sizes (Meigh, 1995; Meigh et al., 1997). Liongson (2004) demonstrated a significant relationship between catchment area and mean annual flood (Q_{MAF}) for 29 sites in northern Luzon, and analysed the form of growth curves. Regional differences in climate and precipitation patterns are well-documented (Bagtasa, 2017) and projections have been made of climate change impacts on river flow (Tolentino et al., 2016) with some evidence for significant changes having occurred in recent decades (Meigh, 1995). Calibrating local data with global runoff datasets enables the augmentation of catchment-specific data to a certain extent (Ibarra et al 2021).

Studies of flood magnitude across South-East Asia provide valuable regional context for our Philippines analysis. Loebis (2002) found significant correlations between mean annual flood and catchment area in Indonesia, Laos and Thailand, as did Meigh et al. (1997) for Indonesia, Papua New Guinea and Thailand. Mamun et al. (2011) provide updated equations for peninsular Malaysia which use catchment area and mean annual rainfall as predictors. In these studies, coefficients of determination (R²) values range from 0.5 to 0.9 tending to be higher in smaller regions—countries and where inter-annual rainfall variability is lower: for example, Meigh et al. (1997) report R² values of 0.92 for Papua New Guinea and 0.46 for administrative regions 3-8 in the Philippines.

There are few continuous long river flow records available for the Philippines, but many short (3-35 years) records exist from all regions of across the country. This scarcity of data leads to the Philippines being omitted from databases used for global flow frequency analyses (e.g. Zhao et al., 2021). Pooling of the information from the available records, taking account of climatic variability across the country, forms the basis of the analysis in this paper. The approach uses elements of the UK Flood Estimation Handbook (FEH) methodology (Kjeldsen et al., 2008), adapted to reflect the nature of the river flow and other data that are available. The paper aims to evaluate the potential of pooling short data series to deliver estimates of flood magnitude for the Philippines. Reliable predictive design equations and frequency that can would then be applied in applicable to ungauged catchments that are ungauged or have short records, and hence to deliver design equations that can be applied across the Philippines.

3 Data sources

Daily mean river discharge data were collated from 842 sites (Table 1) reported by three sources. (1) The "SWS" data set comes from four volumes of the "Surface Water Supply of the Philippine Islands" (Irrigation Division, 1923-24) contain rating curves and daily flow measurements over the period 1908 – 1922. Water level measurements were made at constructed weirs and rating curves were computed using discharges obtained by the velocity-area method. Rating information is supported by detailed information on the measurement site, bank and bed characteristics and river channel stability. Data from 248 SWS stations across the country (Figure 1) were

105

110

115

used. (2) The second dataset ("BRS") was initially managed by the Bureau of Research Standards, later being transferred to the Bureau of Design, also under the Department of Public Works and Highways (DPWH). The BRS data set (Figure 1) is in three parts: BRS_A contains 364 gauging sites with data in the period 1940-1980, BRS_B has a further 181 with data from 1980 onwards. BRS_C includes 27 of the sites from BRS_A and BRS_B that are either at identical locations or are sufficiently close (within a few km, without any significant tributaries in between) to allow for their records to be combined. This produces a maximum record length of 62 years. Some of these sites had automated water level sensors but most sites had a gauging structure at which manual observations were made three times per day. Rating curves were obtained by velocity-area gauging. (3) The source of the third dataset ("Cagayan") is the "Feasibility Study of the Flood Control Project for the Lower Cagayan River in the Republic of the Philippines" produced by Nippon Koei Co. and Nikken Consultants Inc. in collaboration with the DPWH in 2002 (Nippon Koei, 2002). This study only considers the Cagayan watershed, north Luzon, the largest catchment in the Philippines. Out of 78 gauging stations in the watershed, 48 stations (Figure 1) were used in this study since some of the stations only reported gauge height data and others have a lot of gaps. Daily mean water level data were recorded from 1955 to 1991 and converted to discharge using rating curves (details not reported; Nippon Koei, 2002).

The data were initially filtered to remove sites with very short records (<7 years), inadequate rating between water level and discharge and those from the SWS data set where the gauging site location could not be reliably determined. The Philippines has four distinct climate types (Coronas, 1920) shown on Figure 1. For convenience, hydrological data is often reported for 15 administrative regions (Figure S1), and we use this regionalisation to consider whether there is variation in flood hydrology across the country.

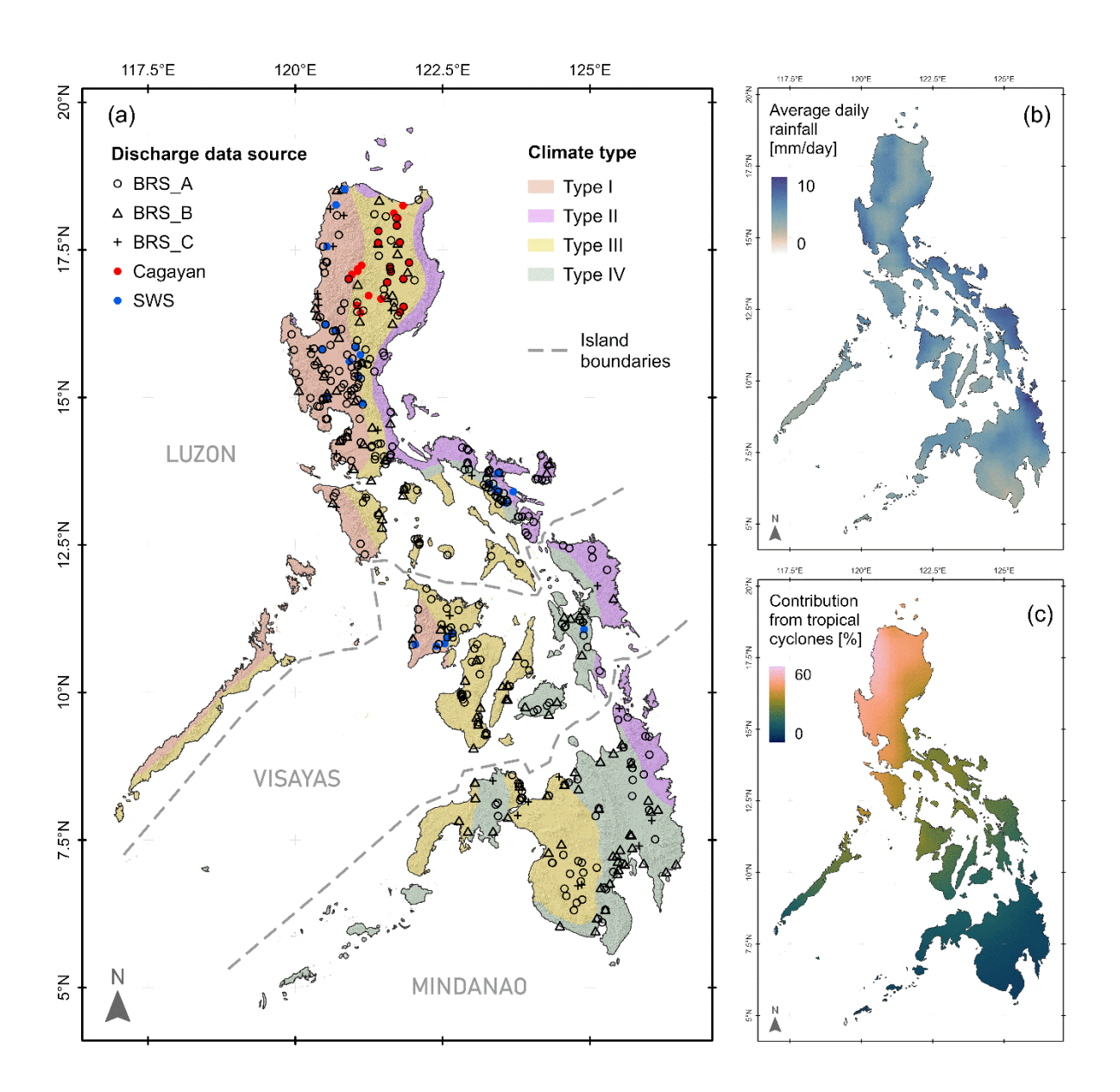


Figure 1: (A) Locations of gauging sites from the data sources used in the analysis (n=466; Table 2). Background map (after Tolentino et al., 2016) shows elevation shading overlain by the four climate types that have been identified for the Philippines (Coronas, 1920). (B) Mean daily rainfall (after Bagtasa, 2017). (C) Proportion of annual rainfall generated by tropical cyclones (after Bagtasa, 2017). The climates can be summarised as (Ibarra et al., 2021): type I -distinct wet and dry seasons; type II - no distinct dry season and relatively high rainfall; type
 III – lower overall rainfall with short dry and wet seasons; and, type IV - reasonably even distribution with lower total rainfall.

Table 1 Summary of available discharge data sets. Candidate sites are sites retained after removing sites with no or poor rating, or indeterminate locations. Record length is the number of years for which reliable annual maximum flow estimates exist, after removal of erroneous data.

Source	Time period of data	Total number of sites	Number of candidate sites	Number of candidate sites with ≥7 years record	Record Length (years) for sites with ≥7 years data (figures in brackets are for all candidate sites)		(figures in
					Max	Mean	Total
SWS	1908 - 1922	248	119	30	10	7.7 (5.1)	230 (604)
BRS_A	1940 - 1980	364	337	310	34	18.3 (17.1)	5659 (5771)
BRS_B	1980 - 2018	154	144	115	33	16.1 (13.9)	1856 (2003)
BRS_C	1940 - 2018	27	27	27	62	36.2 (36.2)	978 (978)
Cagayan	1955 - 1991	49	46	31	20	11.6 (9.5)	361 (437)
TOTAL		842	673	513	62	17.7 (14.6)	9084 (9793)

145

165

4 Analysis Methods

4.1 Curve fitting for annual daily maximum flows

The maximum flows in each calendar year were extracted from the daily flow data and fitted with three distributions: (1) Generalised Logistic Distribution (GLO) (Kjeldsen and Jones, 2006; Kjeldsen, 2013); (2) Weibull; (3) Log-Pearson Type III. The median annual flood (Qmed) was used as the index flood, rather than the mean, to minimise the effect of outliers in the data (Kjeldsen and Jones, 2006), and the parameters of the distributions were estimated using L-moments (Hosking, 1990; Hosking and Wallis, 1997). L-moments are linear combinations of probability-weighted moments, and the GLO distribution uses ratios between the first three L-moments, l_1 , l_2 and l_3 , to define the L-CV (coefficient of variation) t_2 and L-Skewness t_3 as:

150
$$t_2 = l_2/l_1$$
 $t_3 = l_3/l_2$ (1).

The GLO is a three parameter distribution, which has location, scale and shape parameters. The location (ξ) is the median of the distribution. The shape (κ) and scale (β) parameters are estimated from the L-moment ratios (Eq. 1), as:

$$\hat{\kappa} = -t_3 \qquad \qquad \hat{\beta} = \frac{t_2 \hat{\kappa} \sin(\pi \hat{\kappa})}{\pi \hat{\kappa} \sin(\hat{\kappa} + t_2) - t_2 \sin(\pi \hat{\kappa})}$$
 (2),

where $^{\land}$ indicates an estimate of the distribution parameter. Further details on L-moments and their application to distribution fitting are provided by Hosking and Wallis (1997) and Asquith et al., (2017). The GLO distribution can be used to calculate a flood, Q_T , with a recurrence interval of T years as

$$Q_T = \xi \left[1 + \frac{\beta}{\kappa} (1 - (T - 1)^{-\kappa}) \right] = \xi z_T \tag{3},$$

where z_T is the 'growth curve' at T. The Weibull and Log-Pearson Type III distributions are also three parameter distributions, described fully by Asquith et al. (2017) and Hosking and Wallis (1997) who define the relevant L-moments and parameter calculations. The Gringorten (Cunnane, 1978) plotting position (Eq. (4)) was used,

$$x_i = (i - 0.44)/(n + 0.12)$$
 (4),

where x_i is the *i*th quantile of the distribution, *i* being the rank of the annual maximum flood in a given year, and n the total number of years in the record. This method allows estimation of an event of up to (1.79n + 0.2) years return period (Stedinger et al., 1993). Figure 2 shows typical data sets and curve fits.

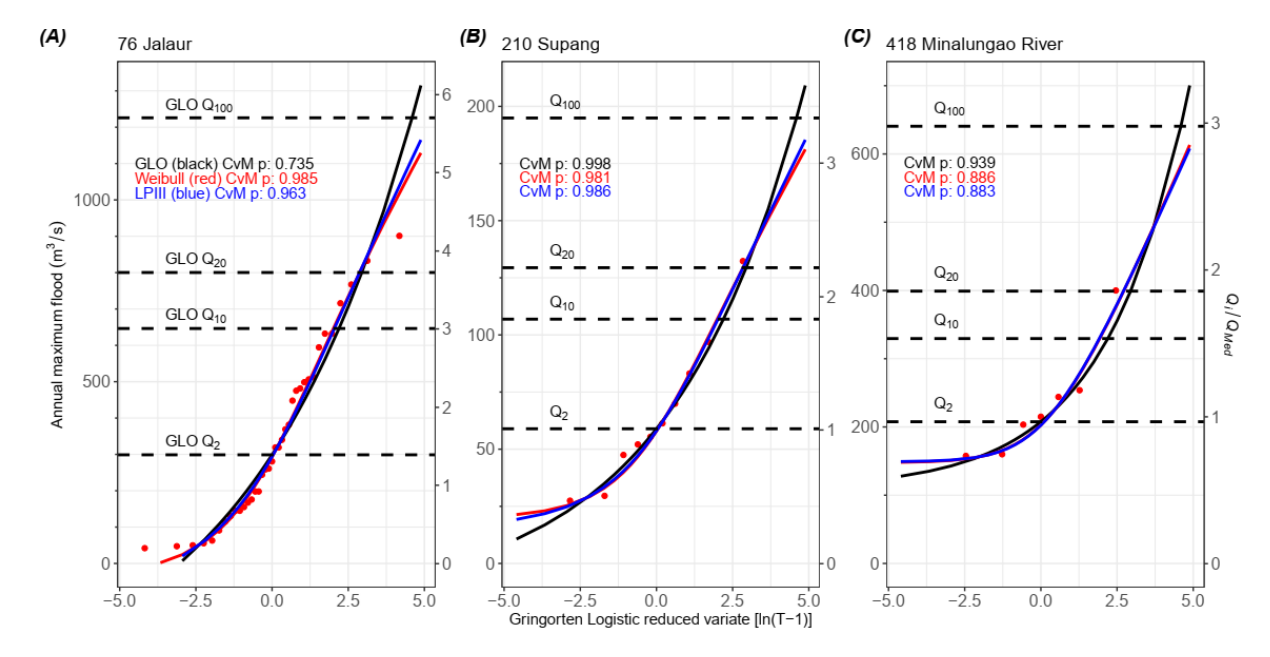


Figure 2: Selected annual maximum flood data and curve fits. Red points are data. Fitted curves are GLO (black), Weibull (red) and Log Pearson III (blue). Craméer-von-Mises p-values shown. Left axes are flood magnitude (m³.s¹) and right axes scale this by the median annual flood at each site. Values of 2,10,20 and 100 year recurrence interval floods are indicated, calculated using the GLO method. (A) Site 76, Jalaur (Lat: 11.1195; Long: 122.5386; Area 210km²; BRS_C data set; 37 years of data; best-fit curve: Weibull); (B) Site 210, Supang (Lat: 17.0073; Long:120.9086; Area 56km²; Cagayan data set; 10 years; GLO); (C) Minalungao (or Sumacbao) River (Lat: 15.3430; Long: 121.0794; Area 309 km²; SWS data set; 7 years; GLO).

Analysis was undertaken in R (R Core Team, 2021), using the package Imomco (Asquith, 2020) to derive the L-moment estimates, to fit the distributions and to calculate their significance. Of the 513 sites with records of at least 7 years length (Table 1), the minimum required for L-moment calculation, two had invalid L-moments and so are excluded from further analysis. For these remaining 5113 sites, goodness-of-fit between the data and the three distributions was assessed using Cramér-von Mises (CvM) test (Asquith, 2020). Such goodness-of-fit tests are unable to definitively identify the best distribution to use, or if any of the distributions are adequate (Asquith, 2020), particularly with relatively short records, as used here. Rather, the CvM p-values provide an indication of the performance of the three distributions. The annual maximum series and the three curve fits were inspected for each site and those with very poor fits were excluded. Mostly these excluded sites corresponded with low CvM p-values, although this was not always the case. The distribution with the highest p-value from the CvM test was used to provide Q_x estimates for the site. This screening process led to the elimination of a further 45205 sites from the data set, leaving 466 that were further analysed. The distribution of the best-fit curves (Table 2) does not show systematic differences between data source, catchment area or climate type (Table 2).

205

220

225

Table 2 Best-fit curves, defined as those with highest Cramér-von Mises test p-value. 207 sites were excluded from the analysis, 2 due to L-moments not being valid, and the remainder due to having short records (<7 years) or a poor curve fit-overall, based on the p-value and visual inspection.

Best fit	All	Data	Source	9		Catchment Area (km²)			Climate Type			oe	
curve	sites	BRS	Cag	SWS	<100	100-	200-	400-	≥800	I	II	III	IV
		A/B/C				199	399	799					
GLO	184	99/52/6	13	14	58	39	31	21	35	48	21	66	49
Weibull	207	131/42/18	8	8	75	42	26	35	29	58	22	86	41
Log	75	52/14/3	3	3	31	8	18	7	11	15	10	37	13
Pearson III													
TOTAL	466	282/108/27	24	25	164	89	75	63	75	121	53	189	103
Used													
Excluded -	205	55/36/0	20	94	66	48	33	19	39	83	8	79	35
poor curve													
fit <u>or < 7</u>													
years data													
L-	2	0	2	0	0	0	1	0	1	0	0	2	0
moments													
not valid													
TOTAL	673	337/144/27	46	119	230	137	109	82	115	204	61	270	138

Values of Q_2 , Q_{10} and Q_{100} were calculated from the fitted curves although the lengths of available records mean that estimates of Q_{100} are subject to significant uncertainty. Towards the high flow end of the data, the Weibull and Log-Pearson Type III curves are usually very similar, with the GLO curve typically being steeper and more curved (Figure 2) and so providing higher flow estimates for high recurrence intervals (Q_{20} , Q_{100}) than the other two curves and often slightly lower estimates of Q_2 and Q_{10} . Ratios between flow estimates from different curves (Figure S1) show this pattern: mean ratios between estimates from the GLO and Weibull distributions are $Q_{2GLO}/Q_{2Wei} = 1.07$ (range 0.99 - 3.48), $Q_{10GLO}/Q_{10Wei} = 0.92$ (0.70-1.00) and $Q_{100GLO}/Q_{100Wei} = 1.09$ (0.42-1.15). Equivalent ratios for the GLO and Log-Pearson Type III curves are $Q_{2GLO}/Q_{2LPIII} = 1.10$ (1.00 - 4.27), $Q_{10GLO}/Q_{10LPIII} = 0.91$ (0.55 - 0.99) and $Q_{100GLO}/Q_{100LPIII} = 1.09$ (0.36-1.15). These ratios show some systematic differences between the distributions (Figures 2, S1) and suggest that the choice of distribution influences flow estimates.

Estimating uncertainty in the Q_x estimates is not straightforward (Kjeldsen, 2013; Kjeldsen and Jones, 2004) and reflects variability in the index flood, in the growth curve and in covariance between the index flood and the growth curve (Kjeldsen and Jones, 2004). For a single site, the factorial standard error for the GLO distribution, fse, is defined as (Kjeldsen, 2013):

$$fse = e^{\left(\frac{2\beta}{\sqrt{n}}\right)} \tag{5}$$

where *n* is the number of annual maxima in the data set. However, dDerivation of Eq. (5) relies on approximations that limit the reliability of the equation when $n \le 20$ (Kjeldsen, 2013). On account of this, *fse* values were calculated only for records of at least 20 years length, all but one of which come from the BRS data sets (Table 1).

Growth curves were calculated for each of the 466 sites (Table 2), using Eq.(3) and equivalents for the Weibull and Log-Pearson Type III distributions, over the range of $-3.5 \le \text{Ln}(T-1) \le 5.0$, i.e. return period T in the range 1 to 149 years. Curves were standardised by dividing discharge by the median annual flood recorded at each site.

Combined growth curves using data from sets of catchments that are adjacent or which have similar properties (eg.e.g. catchment area) can be used to provide estimates of the magnitude of floods of specified recurrence intervals given an initial value for *Qmed*. There are several ways to construct such pooled growth curves for: (i) each of the administrative regions of the Philippines; (ii) each of the four climate types (Figure-1); and, (iii) for catchments of different areas, as identified in Table 2. Firstly, the curves from each site within any of these groups can be combined, by calculating their mean, mean weighted by record length, or median (Figs. S2-S4). Secondly, the data can be amalgamated for all sites within each group and GLO curves fitted to the pooled data. The median and weighted mean methods lead to under-estimation of the longest recurrence interval floods (Figs. S2-S4)

235

240

whereas both the mean of GLO curves from each site and the GLO curves fitted to the amalgamated data increase more rapidly at long recurrence intervals. Note that the variability between sites within a region (or climate type or within catchments of similar area) provides an indication of the uncertainty to be expected when using regionalised curves.

4.2 Predicting high magnitude floods from catchment properties

The values of Q_T provided by the GLO-best-fit curves for each site individually analysis previously determined above, were correlated with catchment properties. To apply the FEH approach described earlier (Kjeldsen et al., 2008), These catchment properties, precipitation and land use were derived from a range of data sources. Table 3 summarises the variables used and provides a comparison with the FEH method (Kjeldsen et al., 2008). Note that much of the data used are not contemporary and significant changes in some variables, particularly land use but potentially also precipitation (Bagtasa, 2017), may have occurred since the SWS data were collected in the early 20^{th} Century.

Table 3. Variables used in the flood prediction analysis.

FEH variable name	Units	FEH Definition	Philippines data equivalent	Variable names (this paper)
AREA	km ²	Catchment area	Area from DEM of the catchment, calculated in ArcGIS	AREA
BFIHOST	-	Baseflow index from soil data	Excluded	-
DPLBAR	km	Drainage path length	Mean average drainage path length to catchment outlet for all segments of the stream network	DPLBAR
DPSBAR	m.km ⁻¹ (FEH) m.m ⁻¹ (this study)	Mean catchment slope	Mean average drainage path slope for all segments of the stream network	DPSBAR
EVAP	mm	Average annual potential evaporation	Excluded	-
FARL	-	Flood attenuation index (lakes etc)	Percentage/proportion of catchment area occupied by attenuation features (inland waters and fishing ponds)	ATT
FPEXT	-	Floodplain extent	Excluded	-
PRAT	none (FEH) mm (this study)	Ratio of P ₁₀₀ /P ₂ for 1-day rainfall	Standard deviation of annual rainfall within the catchment from mean annual rainfall (1998-2015) APHRODITE dataset	RFSD
PROPWET	-	Proportion of time when soil moisture deficit <6mm	Excluded	-
RMED	mm	Median annual maximum 1-day rainfall	Mean of maximum daily rainfall within the catchment from maximum daily rainfall (1998-2015) APHRODITE dataset	RMED
SAAR	mm	Annual mean rainfall 1961-90	Mean of annual rainfall within the catchment from mean annual rainfall (1998-2015) APHRODITE dataset	SAAR
URBEXT2000	-	Proportion of urban land cover in 2000	Percentage of catchment area occupied by urban features (built-up)	URB
None	-	-	Percentage of catchment area occupied by agriculture (annual crop, fallow plus perennial crop)	AG
None	-	-	Percentage of catchment area occupied by closed and open forest	FOR

Page 9

National-scale catchment physical properties for the Philippines were previously calculated and are available as an open access geodatabase (Boothroyd et al., 2023). In brief, topographic analysis was undertaken using a digital elevation model (DEM) acquired in 2013 with a 5 m spatial resolution and 1 m root-mean-square error vertical accuracy (Grafil and Castro, 2014). The DEM was resampled to a 30 m spatial resolution in ArcGIS due to processing constraints. Here, AREA, DPLBAR and DPSBAR were extracted from the geodatabase. Rainfall data were from the end-of-the-day adjusted version of the APHRODITE data set (V1901, Yatagai et al., 2012). Land use variables (ATT, URB, AG, FOR) were from the National Mapping and Resource Information Authority (NAMRIA) 2010 land cover data set (www.namria.gov.ph).

5 Results

5.1 Flood magnitude estimation Validity of L-moment calculations

The L-moment ratio diagram (Figure 3; Figure S6) shows the relationship between L-skew and L-kurtosis differentiated by <u>climate type-catchment area</u> and the optimal best-fit curve. Sites where each of the distribution types fit the data best do cluster close to the theoretical relationships for each of those distributions as expected. Neither climate type (Figure 3), data source, catchment area nor record length (Figure S6) show significant segregation on the L-moment diagram. Consequently, the 466 retained sites are considered as a single data set in subsequent analysis.

270

275

Only for sites (N=71) that had at least 20 annual maxima and for which the GLO distribution provided the best fit to the data, it was possible to compute T_t for factorial standard error (f_se) was computed using Eg. 5 for 71 sites with at least 20 annual maxima and for which the GLO distribution provided the best fit to the data. The values of f_se range from 1.03 to 1.32, with mean = 1.18.

5.2 Regional annual maximum daily flow growth curves

Growth curves for all sites (Figure 4a) show considerable variability within and between regions, reflecting the number, length and quality of available data records as well as catchment properties. To assess variation across the country, we use the administrative division of the Philippines into 15 regions (Figure S1) which are aligned to hydrological and topographic patterns (Figure 1). Different climate zones (Figure 4b) and catchment areas (Figure

295

300

280

4c) indicate some grouping which may form the basis for hydrologic regionalisation. Climate types II and III plot higher than the others (Figure 4b), although the median growth curves for all four climate types are very similar (Figure 4d). The pooled data provide steeper growth curves, reflecting the larger data series used and the increasing influence of large events in these larger samples. Consequently, the pooled data curves match high percentiles of the individual curves (shown by plotting close to, or sometimes outside of, the 75th percentile limits shown in Figure 4b,c). The steeper curves for pooled data are also seen when grouped according to catchment area (Figure 4e). Small ($< 25 \text{ km}^2$) catchments plot separately from all larger areas, and there is little differentiation between any larger catchments. This contrasts with Meigh's (1995) results which suggested a steady decrease in Q_x/Q_{mean} as catchment size increased.

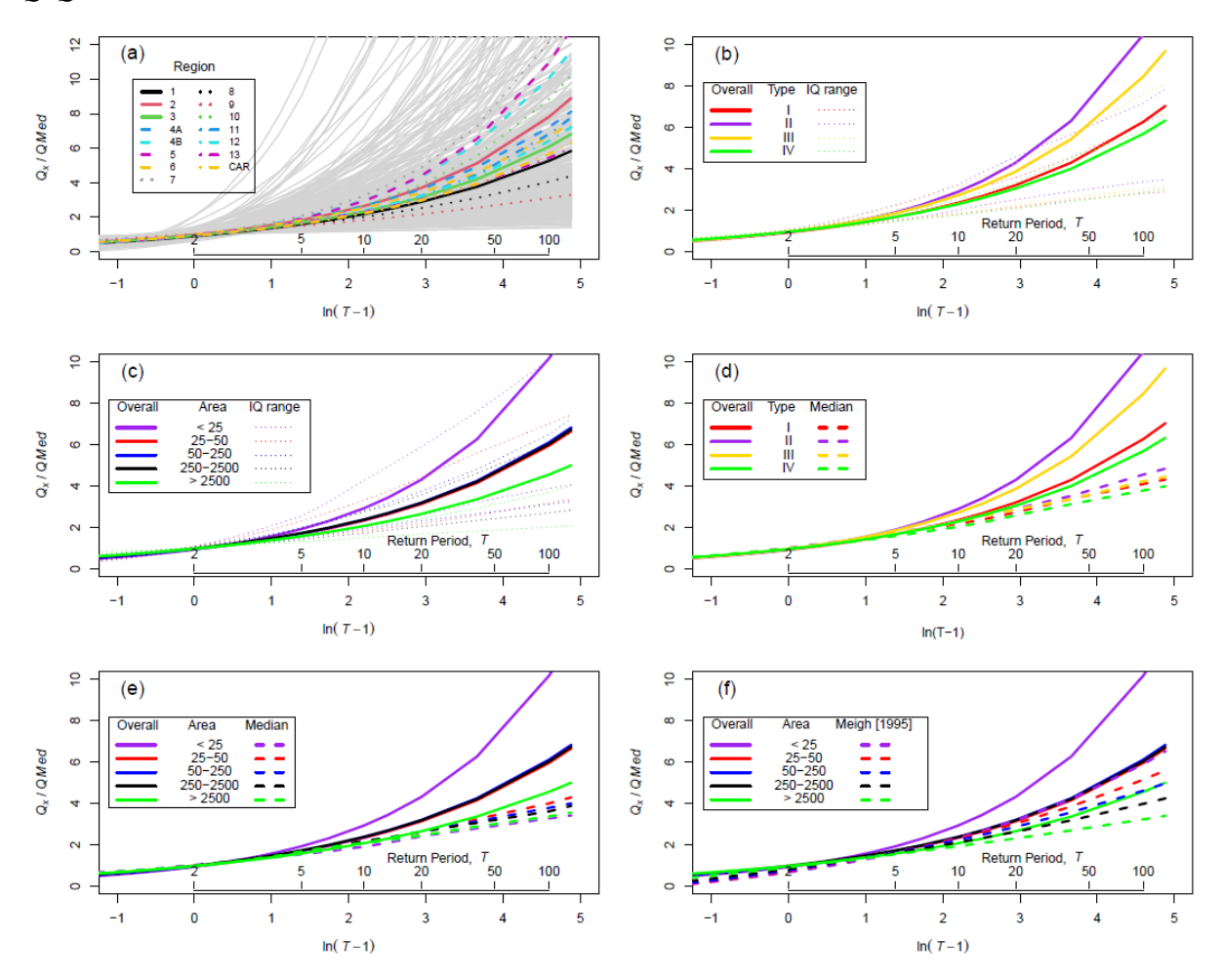


Figure 4 Dimensionless growth curves. (a) individual curves for 466 sites, overlain by pooled curves for each region. (b) GLO curves for data pooled from all sites in each climate type; IQ range lines are the inter-quartile (25th and 75th percentiles) of the curves for individual sites within each climate zone. (c) GLO curves from bins of catchment area, with inter-quartile ranges from individual sites shown. (d) Comparison of GLO curves fitted to all data from within each climate zone and the median value from individual sites within that zone. (e) Comparison of GLO curves fitted to all data for sites within each catchment area bin and the median value from individual sites within that area bin. (f) Overall GLO curves for each catchment area bin, and adjusted equivalent curves from Meigh (1995). Adjustment was necessary as Meigh (1995) used the mean annual flood as the index flood, rather than the median. See text for details.

5.3 Flood estimation equations

5.3.1 Analysis of predictor variables

Each of the variables listed in Table 3, together with the Qx estimates derived in the previous sections, were tested for normality and transformed as required (Table 4). Log10 transformation was used as the default, most variables being moderately positively skewed, with square-root transformation for two land-use (areas of attenuation

315

320

325

<u>features and urban land-use</u>) and one rainfall (<u>standard deviation of rainfall</u>) variables that contained numerous zero values—(<u>areas of attenuation features and urban land, and standard deviation of rainfall</u>). Cross-correlation plots and matrices, of the transformed variables where relevant, (Figure S67) show expected autocorrelation between climate variables and no significant non-linear relationships elsewhere in the predictor variables. Note (Table 4) that mean annual rainfall (SAAR) is poorly correlated with each of the *Qx* measures.

Table 4. Summary statistics for variables used in the flood prediction analysis (466 sites). All values in original units, prior to transformation (Trans). Land-use variables expressed as % were converted to proportion (0-1 scale) for analysis. Correlation coefficient, R, significance: * p<0.01. Geometric mean (Geom mean) shown for variables with no zero values. $^+$ one slope of 0.0 excluded when calculating geometric mean. X_T = transformed value of variable X.

Variable (units)	Min / Max	Mean	s.d.	Geom Mean / Median	Trans		R (log	Q_x - X_T)	
(units)	Max			/ Median		Q_{MED}	Q_2	Q_{10}	Q_{100}
AREA (km ²)	1.13 / 27450	656	2040	172 / 163	Log10	0.77*	0.77*	0.74*	0.70*
DPLBAR (km)	0.02 / 245.7	27.2	27.7	18.0 / 18.9	Log10	0.74*	0.74*	0.71*	0.67*
DPSBAR (m.m ⁻¹)	0.00 / 0.145	0.041	0.024	0.034 ⁺ / 0.044	No	0.03	0.03	0.07	0.10
ATT (%)	0/37.0	1.11	2.4	NA / 0.68	$\sqrt{}$	0.34*	0.34*	0.30*	0.28*
RFSD (mm)	0; 444	101	100	NA / 78.0	$\sqrt{}$	0.48*	0.48*	0.47*	0.45*
RMED (mm)	62.5 / 331	172	57.9	161 / 170	No	0.20*	0.20*	0.20*	0.19*
SAAR (mm)	1169 / 3877	2316	475	2269 / 2238	Log10	0.06	0.06	0.05	0.03
URB (%)	0/51.3	1.80	5.1	NA / 0.48	$\sqrt{}$	-0.06	-0.07	-0.07	-0.08
$AG\left(\%\right)$	0 / 100	36.9	27.6	NA / 32.5	No	-0.31*	- 0.31*	- 0.30*	-0.29*
<i>FOR</i> (%)	0 / 86.4	25.9	23.9	NA / 19.2	No	0.28*	0.28*	0.29*	0.29*
Q_{MED}	0.72 / 6029	380	722	132 / 136	Log10	-	1.00*	0.93*	0.59*
Q_2 (m ³ .s ⁻¹)	0.63 / 6211	374	717	131 / 141	Log10	-	-	0.93*	0.61*
$Q_{10} (\mathrm{m}^3.\mathrm{s}^{\text{-}1})$	1.73 / 15230	831	1590	319 / 325	Log10	-	-	-	0.82*
$Q_{100} (\mathrm{m}^3.\mathrm{s}^{\text{-}1})$	3.75 / 91040	1801	5170	632 / 619	Log10	-	-	-	-

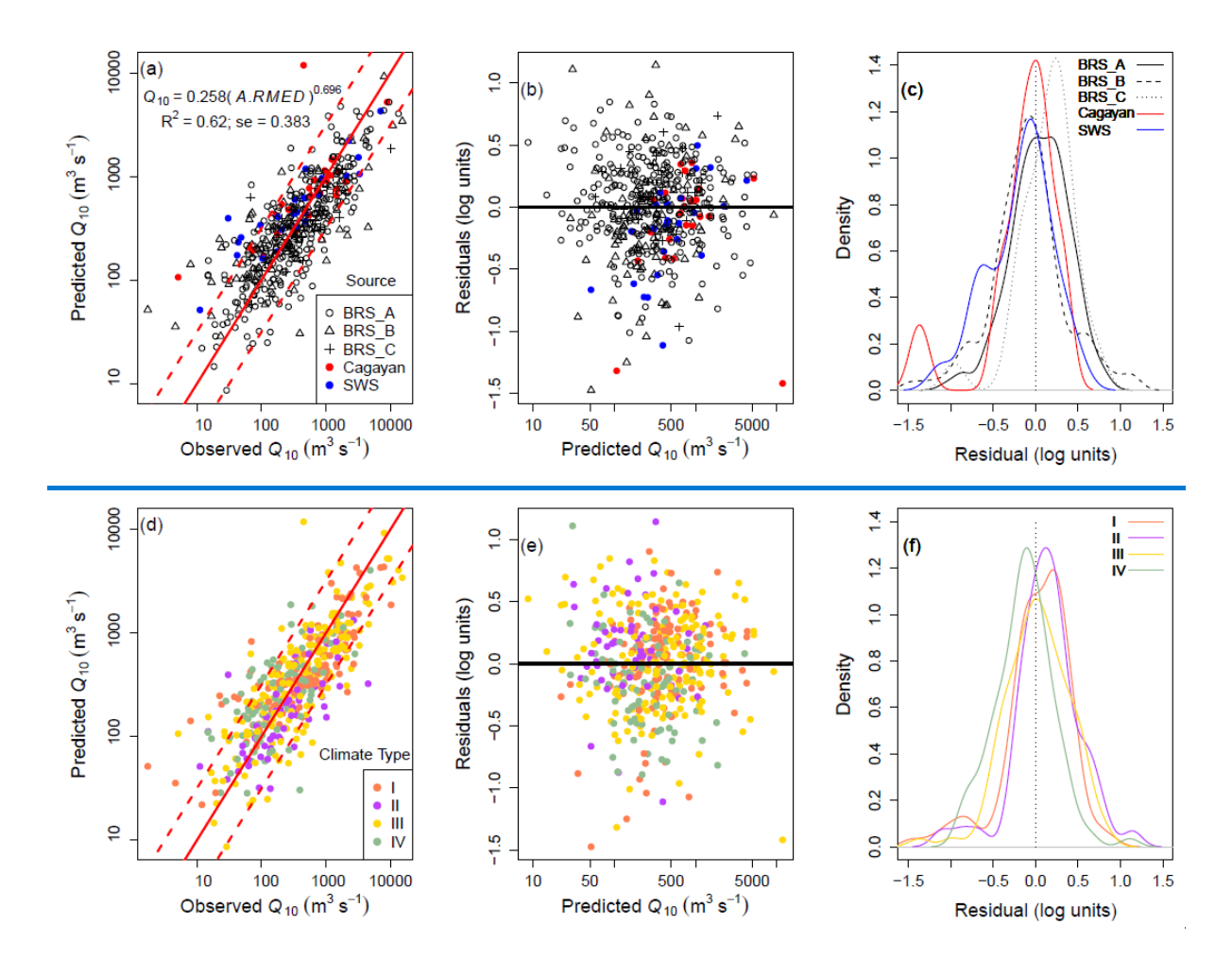
5.3.2 Flood prediction from catchment area and rainfall

The correlations in Table 4 show that catchment area alone provides the most significant prediction of flood magnitude. Drainage path length (*DPLBAR*) provides an equally good predictor as path length and is correlated with catchment area are correlated (Hack's law; Rigon et al., 1996). However, R² for catchment area and *DPLBAR* are in the range 0.45-0.6 so there is potential for additional variables improving flood magnitude prediction. Initially, the rainfall variables were introduced to multiple regression relationships to account for the volume of water entering catchments as catchment area * rainfall. Tables 3 and 4 show two relevant rainfall variables: *SAAR*, the mean annual rainfall and *RMED*, the maximum daily rainfall which serves a measure of the magnitude of rainfall extremes which may be expected to be correlated with flood peaks.

Equations using catchment area alone (Table 5) provide R^2 values between 0.49 (Q_{100}) and 0.6 (Q_2). These rise to 0.55-0.65 when area is multiplied by *RMED* (Table 5). P_{99} , the 99th percentile of daily rainfall, produces equations which fit the data equally as well as *RMED*.

Event return period	Equations	\mathbb{R}^2	se
Q_2	$Q_2 = 3.013A^{0.733}$	0.59	0.424
	$Q_2 = 4.989 \times 10^{-2} (A.RMED)^{0.770}$	0.66	0.387
Q_{10}	$Q_{10} = 10.666A^{0.660}$	0.55	0.417
	$Q_{10} = 2.576 \times 10^{-1} (A.RMED)^{0.696}$	0.62	0.383
Q_{100}	$Q_{100} = 25.645A^{0.622}$	0.49	0.442
	$Q_{100} = 7.568 \times 10^{-1} (A.RMED)^{0.658}$	0.56	0.413

The residuals from the equations using A.RMED as the predictor were examined for effects of data source, climate type or region (Figure 5). One-way ANOVA indicates significant differences between regions for Q_2 , Q_{10} and Q_{100} , with regions 7 (p=0.003; 0.0043; 0.026, respectively), 11 (p=0.012; 0.001; 0.005) and 12 (p<0.001 for all Q_x) being significantly different for all three return periods, region 3 (p=0.02; 0.02) for Q_{10} and Q_{100} , and region 9 (p=0.02) for Q_{100} only. Differences between climate types are only significant for Q_{10} and Q_{100} , in both cases Type IV being significantly different from the others (p<0.01—in—both—cases). For data source, significant differences are noted for Q_2 and Q_{10} , in both cases due to BRS_B (p=0.006 for both) and the early 20th Century SWS (p<0.001; 0.014 for Q_2 , Q_{10} , respectively) data sets. While these results suggest possible benefits from subdividing the data to produce predictive equations, inspection of Figure 5, the boxplots and ANOVA results all show considerable inter-group variance. Hence, the alternative approach of introducing additional variables to the analysis is considered as the next stage of the analysis, before regionalisation is considered in section 5.3.4.



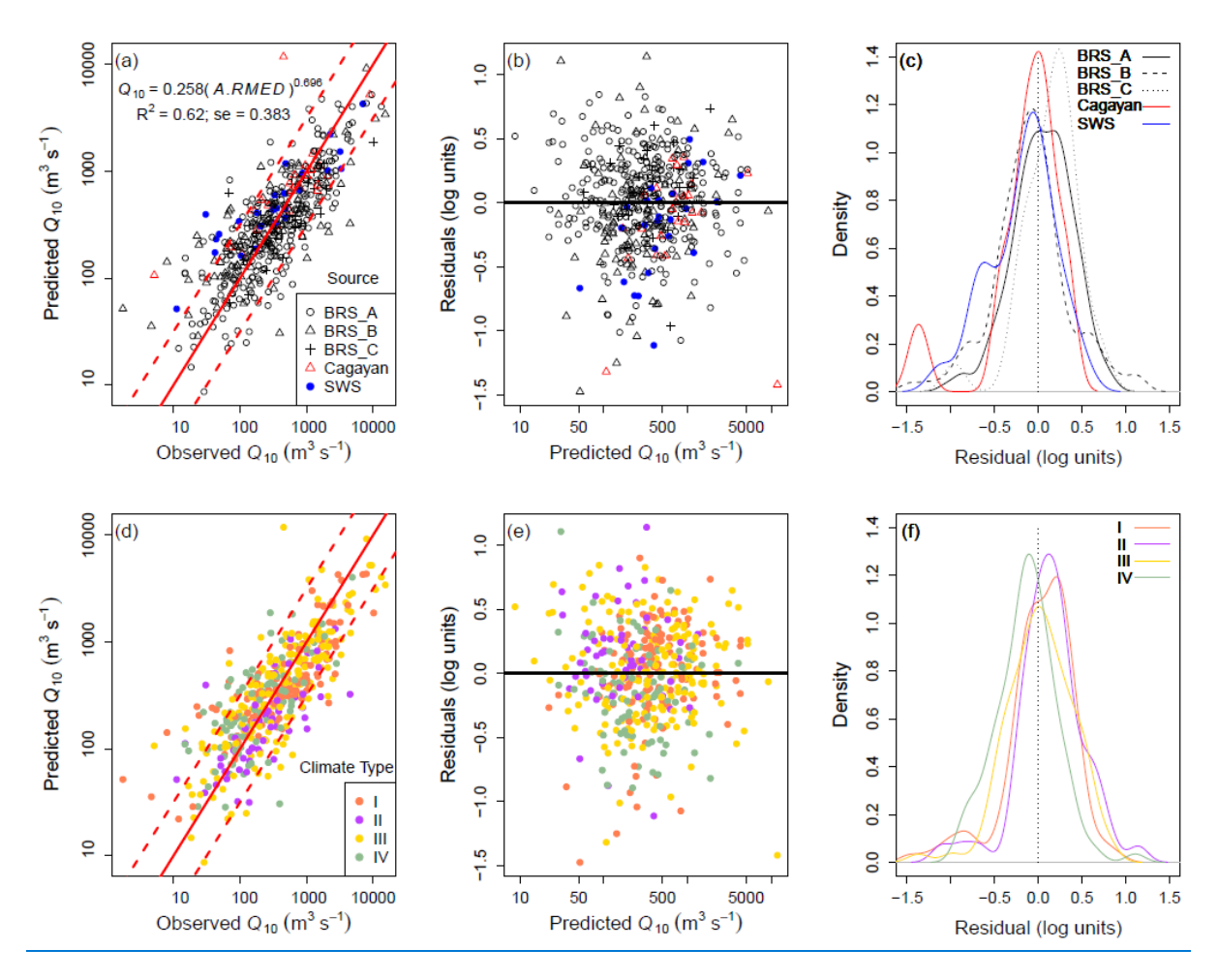


Figure 5. Observed values, prediction and residuals for Q_{10} as a function of catchment area (A) multiplied by median daily maximum rainfall (*RMED*). (a)-(c) stratified by data source, (d)-(f) by climate type. (a),_(d) are predicted vs. observed values, with 1:1 (solid), 1:2 and 2:1 (dashed) lines shown. Residuals (b) and (e) are normally distributed and show no systematic variation with predicted Q_{10} . Density plots of residuals (c), (f) confirm the absence of systematic variation with data source and climate type. Equivalent figures for Q_2 and Q_{100} are in supplementary information (Figs. S78, S98).

5.3.3 Comprehensive stepwise regression prediction

Stepwise regression yielded equations (Eq. 6a eTable 6) with between three and six significant (p<0.05) predictors, but overall R^2 values of 0.68, 0.63 and 0.57 for Q_2 , Q_{10} and Q_{100} , respectively. The modest improvements in R^2 associated with these additional variables suggest that there is limited value in using these complex equations for flood magnitude prediction.

Table 6. Best-fit stepwise equations for the data set covering the whole of the Philippines (n=466). se = standard error of residuals.

Event	<u>Equation</u>	$\underline{\mathbf{R}^2}$	<u>se</u>
return			
period			
<u>Q</u> 2	$8.75 \times 10^{-3} A^{0.753} SAAR^{0.685} 10^{[0.002RMED-2.423DPSBAR-0.165AG-0.676\sqrt{URB}]}$	0.68	0.377
\underline{O}_{10}	$3.44(A)^{0.679}10^{[0.003RMED-0.75\sqrt{URB}]}$	0.63	0.378
<u><i>Q</i></u> 100	$8.49(A)^{0.667}10^{[0.003RMED-0.838\sqrt{URB}-0.673\sqrt{ATT}]}$	<u>0.57</u>	<u>0.407</u>

 $Q_2 = 8.75 \times 10^{-3} \Lambda^{0.753} SAAR^{0.685} 10^{[0.002RMED - 2.423DPSBAR - 0.165AG - 0.676\sqrt{URB}]}$

345

350

370

385

$$Q_{10} = 3.44(A)^{0.679} 10^{\frac{[0.003RMED - 0.75\sqrt{URB}]}{(6b)}}$$

$$Q_{100} = 8.49(A)^{0.667} 10^{\frac{[0.003RMED - 0.838\sqrt{URB} - 0.673\sqrt{ATT}]}{(6c)}}$$

$$[R^2 = 0.57; \text{ rmse} = 0.407] (6c)$$

This limitation is enhanced by consideration of the variables in the equations. Each equation contains land-use variables (ATT,URB,AG) that are determined from modern conditions. The relevance of these values to historical data is uncertain given historic and contemporary land-use change across the Philippines. Their inclusion in equations for all three return periods does suggest that land-use may play a significant role in flood magnitude. In all three cases, AREA enters the equation first, followed by RMED. R^2 values after each of these steps, for Q_2 , Q_{10} and Q_{100} are: AREA 0.59, 0.55, 0.49; and, AREA and RMED 0.66, 0.62, 0.55. Adding further variables (Eq. Table 6) improves R^2 by \leq 0.02, hence only catchment area (AREA) and median annual maximum daily rainfall (RMED) are considered necessary for developing predictive equations. Whether these two predictors are added sequentially or are multiplied together (Table 5) does not affect overall model performance (note that the rmse values quoted in the equations are for the transformed variables). Subsequently, the product AREA.RMED is used as a single measure of flood event rainfall volume across the catchments.

5.3.4 Regionalisation of predictive equations

The dimensionless growth curves (Figure 4a), inspection and ANOVA analysis of regression residuals suggest that regionalisation may be able to improve predictive equations. Although the growth curves also show some segregation between climate types, this is not found to be a significant cause of variation in the residuals from predictive equations. Fitting equations to each region separately (Figure 6a) yields improvement in R² and residual standard error for some regions, but this is inconsistent. The regional equations suggest that some grouping of regions may be beneficial.

Three ways of dividing the 15 regions into groups were considered: (a) classification by visual inspection of the growth curves; (b) K-means cluster analysis of the intercepts (a) and gradients (b) for regression equations (Figure 6a); and, (c) the regionally contiguous groups used by Meigh (1995). Each grouping was tested for Q_2 , Q_{10} and Q_{100} predictions. Results were consistent between these return periods, and results for Q_{10} are given in Table 6-7 (see Supplementary Information for Q_2 and Q_{100} results).

Table 76. Equations for different groups of regions. Results for Q_{10} are presented. Meigh (1995) did not include regions 13 or CAR, so the total number of sites in the three <u>contiguous regional</u> groups is 431.

Group	Regions in group	Number	Equation	\mathbb{R}^2	se
		of sites			
Growth cu	ırve				
A	1,13,CAR	65	$Q_{10} = 0.234(A.RMED)^{0.730}$	0.78	0.245
В	2,3,4A,6,11,12	241	$Q_{10} = 0.0945 (A.RMED)^{0.779}$	0.64	0.390
C	4B,5,7,10	126	$Q_{10} = 1.303(A.RMED)^{0.530}$	0.36	0.427
D	8,9	34	$Q_{10} = 0.628(A.RMED)^{0.603}$	0.69	0.211
K-means o	clustering of regional regre	ession equation	S		
E	1,6,7,8,11	142	$Q_{10} = 0.095(A.RMED)^{0.796}$	0.75	0.298
F	2,3,4A,CAR	167	$Q_{10} = 0.071(A.RMED)^{0.813}$	0.69	0.389
G	4B,9,10,12,13	103	$Q_{10} = 1.24(A.RMED)^{0.534}$	0.50	0.370
Н	5	54	$Q_{10} = 5.10(A.RMED)^{0.388}$	0.19	0.475
Meigh (19	95) contiguous regional g	roups			
I	1,2	86	$Q_{10} = 0.166(A.RMED)^{0.753}$	0.63	0.357
J	3,4A,4B,5,6,7,8	264	$Q_{10} = 0.334(A.RMED)^{0.674}$	0.56	0.402
K	9,10,11,12	81	$Q_{10} = 0.851(A.RMED)^{0.535}$	0.45	0.331

The R^2 and standard errors of residuals in Table $\underline{76}$ are compared with the combined results for all regions in Table 5 ($R^2 = 0.62$; se = 0.383). Weighting both the R^2 and residual error values by the number of sites in each group/region suggested that for Q_2 , Q_{10} and Q_{100} the highest R^2 values are those obtained using the overall regressions on the full data set (Table 5). The residual standard errors are slightly lower when obtained from the 15 individual regional curves (0.36, 0.35, 0.37 for Q_2 , Q_{10} and Q_{100} , respectively) than from the overall regressions (0.39, 0.38, 0.41). However, these differences are small and there is insufficient evidence to justify use of either curves for individual regions or groups of regions.

390

405

410

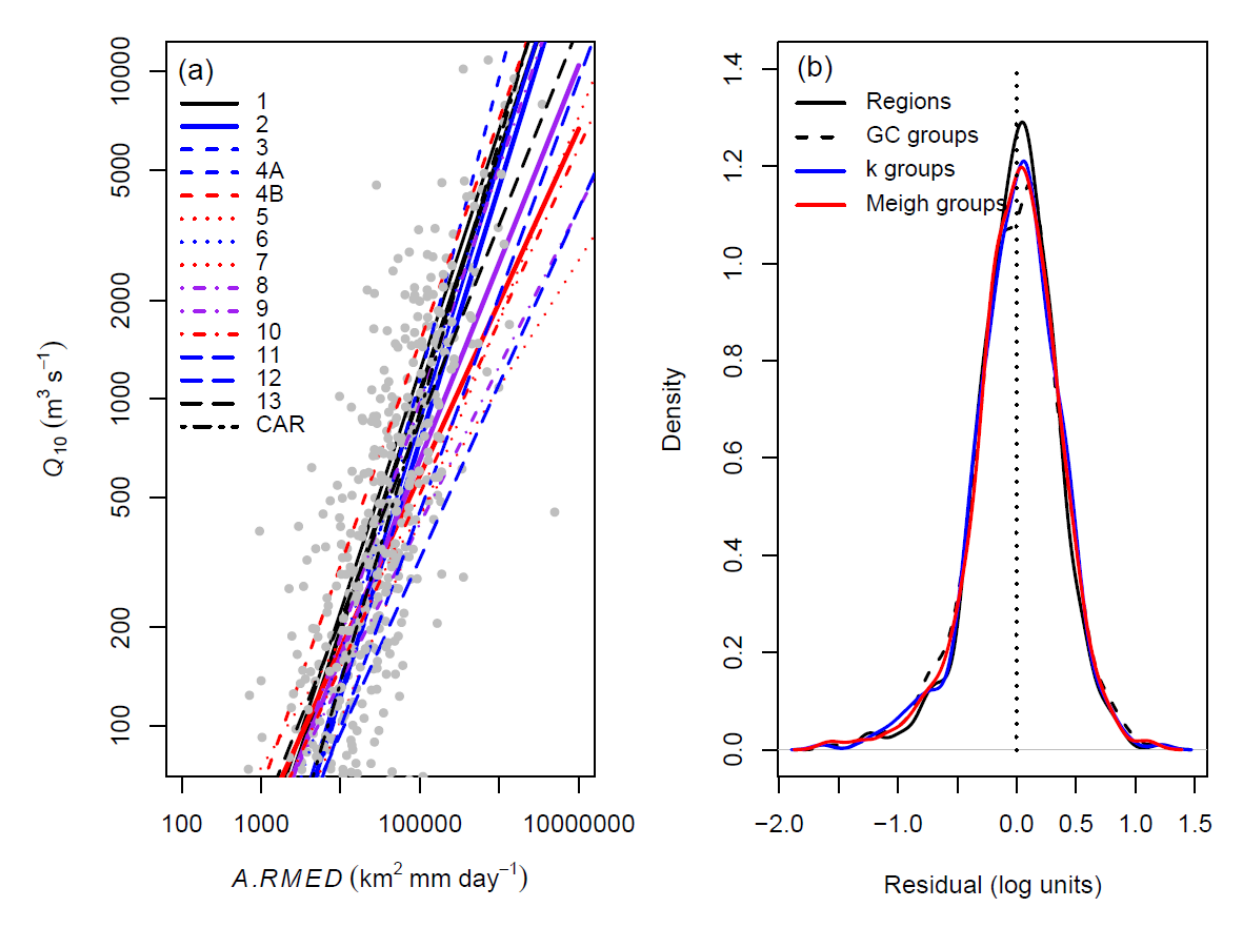


Figure 6. (a) Regression curves for each region in the form $Q_{10} = a$ (A.RMED)^b. Curves are grouped according to growth curve shapes (Table 76): group A (black), B (blue), C (red) and D (purple), and bold lines are regional curves given by the equations in Table 76. (b) Probability density functions for residuals from the individual regional curves in (a), and the three groupings of regions in Table 67 (GC = Growth Curve; k = k-means). Note the similarity in the distributions of residuals, although those for the individual regions are clustered slightly more closely around the mean than those from the grouping methods.

5.3.5 Spatial distribution of flood magnitudes and residuals

The spatial distribution of calculated specific flood magnitudes (Q_{xx} divided by catchment area A) (Figure 7a) show a concentration of higher values through the central Philippines, with relatively lower values in NE Luzon and across Mindinao in the south. The underlying annual rainfall map shows a general decline from east to west, and some of the highest rainfall areas are associated with high Q_{xx}/A values, for example in the Bicol region. Residuals from the overall equations (Table 5) do not show strong regional trends, although there are clusters of positive and negative residuals in different regions. The residuals are not correlated with catchment area (R = 0.04; p = 0.39) and only weakly with annual rainfall (R = 0.15; P < 0.001). However, there is a significant positive correlation between residuals and specific flood magnitude (R = 0.62; $P < 2 \times 10^{-16}$), with only negative residuals for $Q_{10}/A < 0.46$ and only positive residuals when $Q_{10}/A > 6.4$. These results are replicated for Q_2 and Q_{100} , with significant correlations of 0.6 ($P < 2 \times 10^{-16}$) for both Q_2/A and Q_{100}/A).

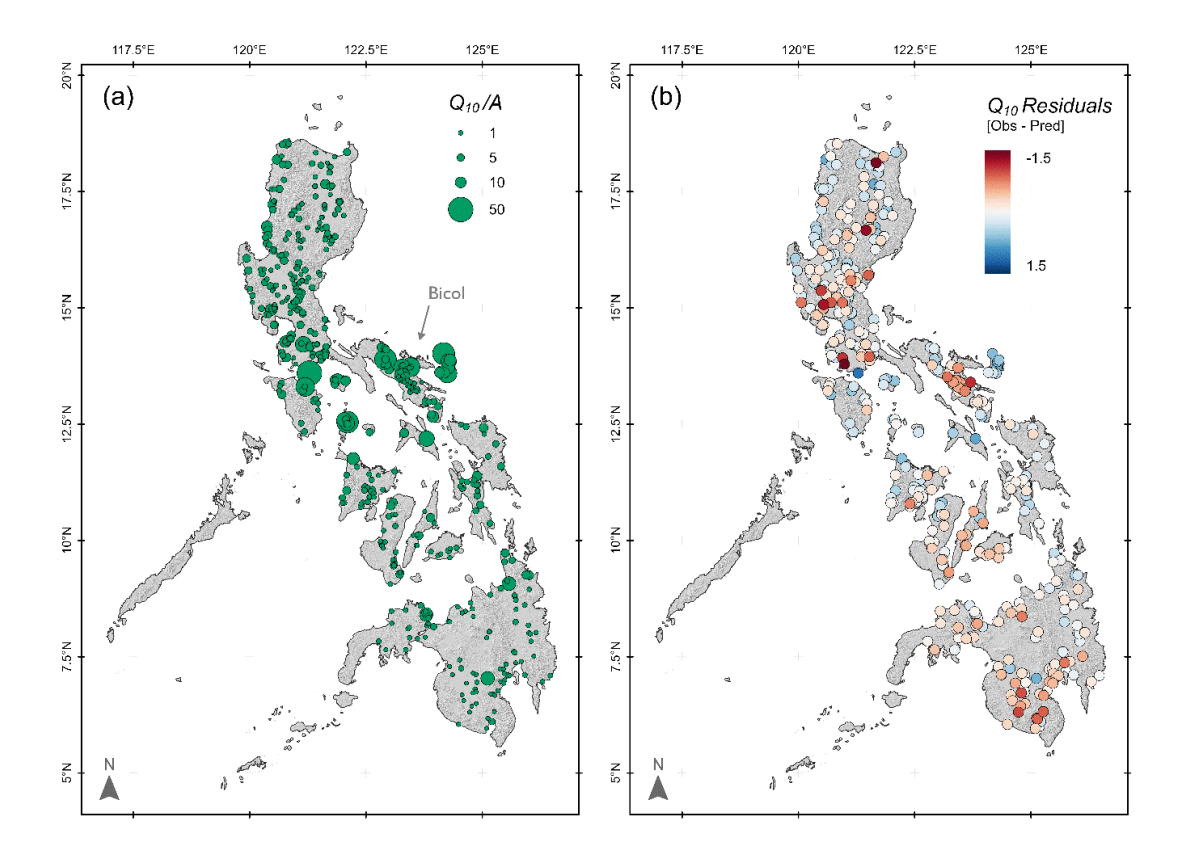


Figure 7. (a) Specific 10-year flood discharge (Q_{10}/A) , showing generally higher values in the central Philippines and southern Luzon, and lower values across Mindanao. (b) Residuals (in log10 units) from Philippines-wide (Table 5) equations for Q_{10} . Note the absence of regional trends, although there are some sub-regional clusters of both positive and negative residuals.

6 Discussion

415

420

425

430

435

6.1 Design equations for the Philippines

6.1.1 Data availability and quality

Flow data were combined from four data sets that are partly independent, having been collected by different agencies and using different methods, but which overlap significantly in collecting data at the same or nearby locations. Catchment properties, such as area and gradients, were derived from a high_resolution DEM that covers the whole of the Philippines. Although some station locations are ambiguous in the data records, the locations of all stations included in the analysis have been reliably identified using the descriptions in the original data sources. Land use data rely on a single time, and no historical land use data are available. This introduces uncertainty to the analysis, especially for data collected a century or more prior to the land use data in areas that have undergone urban development orand forest replacement by agriculture.

The proportions of variance in flood estimates that are statistically explained by the best-fit equations (R²; Tables 5-7,6; Eq. 6) are within the range from studies in other tropical regions (Meigh et al., 1997), from 0.38 (Malawi) to 0.92 (Papua New Guinea). The relatively low R² values reflect a range of factors, including: data quality and length of flow records; changing climate and hydrological conditions during the time period covered by the study; and, controls over flood magnitude in these tropical catchments being influenced by hydrological parameters that are not considered in the analysis. Data quality has been assessed throughout, with sites excluded if their growth curves are based on short records or do not fit expected shapes (Tables 1,2). Further, there is no evidence of bias in the data, shown both by the original variables and the behaviour of residuals from the final predictive curves. For example, the best-fit curves are not biased by data source, climate type or record length (Figures 3; S6,S8,S9). The residuals show neither systematic variation across these same categories (Figure 5) nor consistent spatial dependence (Figure 7).

Some spatial dependence is visible in Figure 7, although attempts to produce regionally consistent predictive curves (Table 67; Figure 6) do not improve the overall performance of the equations compared with national equations. The residuals in Figure 7 do not correlate clearly with either total rainfall (Figure 1B) or the relative importance of tropical cyclones in generating precipitation (Figure 1C). Further analysis of the role of regional climate in flood generation may be able to provide some improvements to predictions, although this is complicated by ongoing climate change and potential changes in the importance of cyclonic precipitation (Bagtasa, 2017).

6.1.2 Recommended design equations

Neither the addition of further catchment variables (Eq. 6), nor regionalisation (Table 76) generated significant improvement in the predictive capabilities of the discharge equations. Hence, it is recommended that single national equations are utilised. This approach has the advantage of maximising the size of the data set used in generating the equations; particularly for the largest catchments, the small sample size reduces confidence in the predictions in some regions. Regionally grouped equations (Table 76) can provide additional estimates of flood magnitude that may be helpful in some cases.

The recommended design equations for Q_2 , Q_{10} and Q_{100} are those for the whole of the Philippines given in Table 5. Using only catchment area, A, will provide usable flood magnitude estimates, the uncertainty of which can be estimated from the residual standard errors given in Table 5. Here we obtained *RMED* values from the APHRODITE database. *RMED* can be determined in other ways, and the sensitivity of flood predictions to changing *RMED* can be assessed directly. Along with catchment area, other catchment properties that provide information to contextualise the flood magnitude estimates can be obtained from an open access database (Boothroyd et al., 2023). Utilising design equations based on catchment area alone has the advantage of simplicity of computation, but the relatively low R^2 values (Tables 5,76) obtained suggest that a simple multivariate regression approach offers only partial improvement to the predictive capability of the equations.

Table 8 shows sample calculations for two sites, one of which (Agno) has 19 years of annual maxima available whereas the other (Sumlog) is ungauged. For the Agno, all of the equations from Tables 5 and 6 produce higher estimates of Q_{10} than from the observations. The reliability of the predictive equations may be affected by this being one of the largest catchments in the Philippines. The Sumlog is a smaller catchment for which no data are available. In this case, the equations provide a smaller range, with the calculations using the three regional methods (Table 7) spanning the result from the national-scale equation using A.RMED in Table 5.

Table 8. Sample calculations for Q_{10} using equations from Tables 5 and 6. The six Q_{10} estimates for each site are as follows: Q_{10} (data) from annual maxima recorded at the Agno site only; Q_{10} (A) using catchment area only – equation from Table 5; Q_{10} (A) using catchment area and A (A) using catchment area only – equation from Table 5; Q_{10} (A) using catchment area and A (A) using catchment area only – equation from Table 5; Q_{10} (A) using catchment area and A (A) using catchment area only – equation from Table 5; Q_{10} (A) using

River	<u>Lat.</u>	Long.	Catchment area, A (km ²)	Philippines Admin. Region	RMED (mm)	Number of years of data
Agno	15.81357	120.45855	2432.1	<u>1</u>	185.6	19
Sumlog	6.97505	126.06849	430.0	<u>11</u>	93.55	n/a
	<u>Q₁₀ (data)</u>	<u>Q₁₀ (A)</u>	<u>Q</u> ₁₀ (A.RMED)	<u>Q₁₀ (GC)</u>	<u><i>Q</i>₁₀ (k-means)</u>	<u>Q₁₀ (Meigh)</u>
Agno	1471	1831	<u>2221</u>	3141	3011	3006
Sumlog	n/a	583.6	412.7	365.0	439.5	247.4

6.2 Comparison with other estimates

6.2.1 Comparison with similar approaches

The previous large-scale study of Philippines flood magnitude (Meigh, 1995; Meigh et al., 1997) used a smaller data set than here, based mainly on BRS data from before 1980, and fitted only the General Extreme Value distribution to the annual maxima time series. The overlap in data means that Meigh's (1995) study cannot be considered to be independent of the present analysis and so does not provide a validation of our results. Some comparison between the two studies is valuable to illustrate the effects of using an expanded data set and the GLO

460

450

455

465

470

480

490

495

500

505

510

515

fitting approach (Figure 4f). Liongson (2016) used data from 29 stations and found that $Q_m = 5.90 A^{0.763}$ (R²=0.65), which is consistent with results in Table 5 as Q_m lies between Q_2 and Q_{10} .

Meigh et al. (1997) present global data, although with an emphasis on tropical regions. Their best-fit equations contain few variables, often only catchment area with mean annual rainfall as the secondary predictor. Comparison of equations between sites revealed the expected overall pattern of higher specific discharges in more humid areas with steeper growth curves in more arid locations that have more variable rainfall, as also seen in the data of Loebis (2002). The consistency of rainfall across the Philippines leads to a clear catchment area effect (Figure 4f) in growth curves for small (<25 km²) and large (>2500 km²) catchments, although using aggregated data shows no differentiation for catchments of intermediate sizes. Individual catchment growth curves show considerable variation within all of the catchment area bins, suggesting that caution is needed in using the aggregated curves for predictive purposes at individual sites. Figure 4 provides a range of aggregated growth curves that can be applied according to catchment area and/or climate type. The differences between the median and mean curves on Figure 4 reflect skew in the growth curve distributions, which is likely to result from the use of relatively short records some of which will include long return period events so overestimating flood magnitudes. Median curves (climate type - Figure 4d; catchment area – Figure 4e) can be used in flood estimation, with the associated mean values and inter-quartile ranges (Figure 4b,c) giving indications of the possible variability, and hence uncertainty, associated with these estimates.

6.2.2 Comparison with rainfall-runoff modelling

The Philippines "Nationwide Disaster Risk and Exposure Assessment for Mitigation (DREAM) Program" produced reports for major Philippines river basins (https://dream.upd.edu.ph/products/publications/index.html) that included flood magnitude estimation. In the DREAM study, 24-hour rainfall events with a range of return periods were calculated from data and these events were then used to model river flows in HEC-HMS 3.5 software. Comparisons are made using catchment area equations (Table 5) for Q_{10} and Q_{100} for sites with unambiguous locations from where DREAM results are reported and for which we are able to calculate catchment areas.

 Q_{10} and Q_{100} comparisons (Figures 8a, S10) cluster around the 1:1 line of agreement. The HEC-HMS estimates exceed the predictions using catchment area at 27 of 38 sites for Q_{10} , and at 24 sites for Q_{100} . Mean ratios between HEC-HMS and predicted values are 1.61 for Q_{10} and 1.76 for Q_{100} . The HEC-HMS results are for instantaneous flows which will be greater than the predicted daily mean flows, with the magnitude of this difference depending on hydrograph shape and hence catchment size (Figure 8b). Given the uncertainties in the data and predictions noted above, and the limited calibration data available for the flood modelling in the DREAM project, the results shown in Figure 8 provide confidence in both the HEC-HMS modelling undertaken for the DREAM project and the catchment area_-based predictions developed herein.

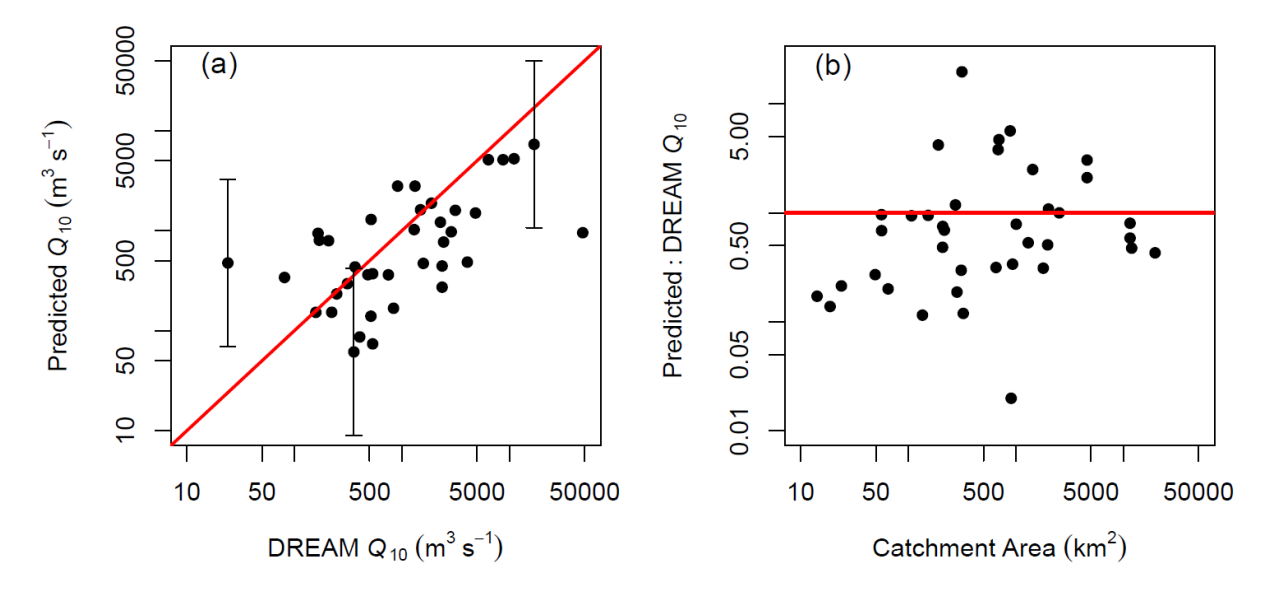


Figure 8. (a) Comparison between Q_{10} estimates based on catchment area (Table 5) and HEC-HMS estimates from the DREAM project. Red line is 1:1 equivalence. (b) Effect of catchment area on the ratio between Q_{10} values from this paper and the DREAM HEC-HMS modelling. Red line shows equal Q_{10} values from both

525

530

535

540

545

550

555

560

565

methods. DREAM estimates are instantaneous peak flows whereas the estimates herein are daily means. As catchment area increases, equivalence between the two methods would show the Q_{10} ratio increasing towards 1.0 as catchment area increases, with lower values in smaller catchments in which flood peaks are of much less than one day duration. 95% prediction intervals are shown for selected points on (a) to indicate the magnitude of statistical uncertainty in the predictions. These are approximated as ± 2 s.e., where s.e. is the regression standard error given in Table 5. Figure S10 presents equivalent results for Q_{100} .

6.3 Combining data from multiple sources

Long hydrological time series are not commonly available worldwide, with particular challenges in developing countries (Cabrera and Lee, 2020). More usually, short, discontinuous records are available and the challenge is to make best use of these to produce regional or national design equations. Combining data from different sources and that was collected over different time periods raises several issues, including: changing data gathering methodologies; climate and land use changes; and, rating curve changes due to relocation of measuring sites and/or river bed morphological change. Uncertainty in individual measurements was assessed here through careful reading of available metadata and quality control. The metadata available for the early 20th Century SWS data includes very detailed site descriptions, rating curves, assessment of site stability and statements on data reliability from the authors (Irrigation Division, 1923-24). Such details are rarely available, at least in accessible public records, for more recent data. The SWS reports provide useful insight into the challenges of hydrometric monitoring in the Philippines, with several sites showing evidence of channel change and frequent shifts in rating curves. Although beyond the scope of this paper, such changes in rating behaviour can be used to assess the impacts of land use and climate changes on river sediment budgets (eg Slater et al., 2015).

The validity of combining data is difficult to assess directly. The residuals from predictive curves (Figure 5c), and similar disaggregation by data source for other parts of the analysis herein, show no significant difference between data sources. This absence of evidence of systematic bias between the data sources supports their aggregation. However, aggregation does need to be undertaken carefully with assessment of data quality and comparability at all stages of the analysis.

6.4 Enhancing the predictions

Tropical cyclones generate many of the significant floods in the northern Philippines, where they contribute over 50% of total rainfall (Figure 1; Bagtasa, 2017), but are very infrequent south of 10°N. Annual rainfall totals show less variability (Figure 1), although rainfall seasonality varies between climate types. Climate models predict increasing flood magnitudes across the Philippines north of 10°N for nearly all scenarios, with smaller or no increases predicted in southern regions (Tolentino et al., 2016).

The existing flow data base, coupled with geospatial information (Boothroyd et al., 2023), can be used for further analysis. Regional spatially-weighted grouping methods (Bocchiola et al., 2003; Griffiths et al., 2020; Muhammad and Lu, 2020) may reveal sub-regional controls over flood magnitude that will be able to improve predictions. Hydrological similarity between catchments does not necessarily imply regional proximity. In the Philippines, climatic gradients are observed both east-west due to topographic influences and north-south as a result of typhoon locations (Figure 1). Coupled with topographic diversity due to the range of island sizes and relief, a range of hydrological characteristics is expected across the country. Hence, statistical grouping (eg clustering, Figure 7) of catchments is necessary to identify hydrologically similar behaviour and provides a more cost-effective and achievable approach than resource-intensive rainfall-runoff modelling (Griffiths et al., 2020). Regional studies from the Philippines have shown the relative contributions that rainfall and topographic factors make to flood magnitude (Cabrera and Lee, 2020) and this approach may be extended nationally.

The methods in this study assume stationarity in the data time series, which has increasingly been questioned as the impacts of recent climate change and a range of anthropogenic factors on flood properties have been observed (Kalai et al., 2020; Kundzewicz et al., 2017). Consequently, approaches that explicitly consider non-stationary time series (eg. François et al., 2019; Kalai et al., 2020) are being developed and refined. Spatially variable responses to changing climate suggest the need for spatio-temporal modelling (Franco-Villoria et al., 2018) and regional calibration of predictive equations (e.g. Griffiths et al., 2020). Our combined data set will enable some of these analyses to be undertaken in the Philippines, so potentially improving the understanding and prediction of flood peaks.

575

580

585

590

600

605

7 Conclusions

Collation of historical data from multiple sources is a widely used technique in climatological and hydrological studies to extend modern records. Changes to data collection methods, to the environment in which the data are collected and to the ways in which data are recorded and reported all affect the reliability of such consolidated data sets. Here we access an extensive and well documented data set from the early 20th Century (SWS data; Irrigation Division 1923-24) that extends annual maximum flood records from the Philippines. The data set is extended from that analysed by Meigh (1995), although the results herein are largely consistent with that study. Recent high-quality supplementary data on catchment properties, precipitation and land use have been added to the analysis enabling assessment of a range of controls over flood magnitude.

Multivariate analysis shows that predictive equations for floods of recurrence intervals from 2 to 100 years based on catchment area alone have R^2 values no greater than 0.59, but that incorporating *RMED*, the median annual maximum 1-day rainfall, as a precipitation variable only increases R^2 to between 0.56 for Q_{100} and 0.66 for Q_2 . Very few other variables were significant when added to multiple regression equations. The relatively low R^2 values are typical of studies from tropical regions, suggesting that the Flood Estimation Handbook approach developed for temperate climates requires some re-design for application to the tropics. The equations developed herein are suitable for use as design equations for the Philippines, but the uncertainties in predictions need to be assessed. Comparison with previous, independent, HEC-HMS modelling is encouraging but serves to illustrate the uncertainties in flood magnitude prediction that remain using either of these methods.

The Philippines exhibits regional climate variability, and there is some spatial structure in residuals from the predictive equations. However, region-specific predictive equations do not perform significantly better than the national equations.

This study demonstrates the potential for combining data from multiple sources to generate flood magnitude predictions. Combining individually short records, after careful screening and exclusion of erroneous data, generates large data sets that can produce consistent results. Enhanced data gathering and extension of continuous flood records are required to reduce uncertainties and improve flood forecasting, but the consistency across the Philippines suggests that extrapolation from a small number of carefully selected catchments could provide nationally reliable predictive equations with uncertainties that are considerably reduced from our results.

8 Data availability Data are available via the University of Glasgow Enlighten Research Data system as Flood estimation for ungauged catchments in the Philippines: Annual Maximum Flow (AMAX) and catchment properties data. Datacite doi:10.5525/gla.researchdata.1666

9 Supplement link: the link to the supplement will be included by Copernicus, if applicable.

10 Author contribution Conceptualisation: TH, EP; Funding acquisition: RW, EP, TH; Methodology: TH; Investigation: TH, PT, EG, RB; Writing Original Draft: TH; Writing – Review and Editing: RW, PT, RW, RB, CD, EP

11 The authors declare that they have no conflict of interest.

12 Acknowledgements Funding was through grants from the Newton Fund of the UK Natural Environment Research Council (NERC; NE/S003312) and the Department of Science and Technology - Philippine Council for Industry, Energy and Emerging Technology Research and Development (DOST-PCIEERD), and from the Scottish Funding Council Global Challenges Research Fund. PMLT is in receipt of a DOST-Science Education Institute (DOST-SEI) and British Council award.

13 References

Asquith, W.: Package 'lmomco'. https://cran.r-project.org/web/packages/lmomco/, 2020.

Asquith, W.H., Kiang, J.E. and Cohn, T.A.: Application of at-site peak-streamflow frequency analyses for very low annual exceedance probabilities, U.S. Geological Survey Scientific Investigation Report 2017-5038, https://doi.org/10.3133/sir20175038, 2017.

Bagtasa, G.: Contribution of tropical cyclones to rainfall in the Philippines, J. Climate, 30, 3621-33, https://doi.org/10.1175/JCLI-D-16-0150.1, 2017.

- Bocchiola, D., De Michele, C. and Rosso, R., Review of recent advances in index flood estimation, Hydrol. Earth Syst. Sci., 7, 283-96, https://doi.org/10.5194/hess-7-283-2003, 2003.
- Boothroyd, R.J., Williams, R.D., Hoey, T.B., MacDonell, C., Tolentino, P.M.L., Quick, L., Guardian, E.L., Reyes, J.C.M.O., Sabillo, C.J., Perez, J.E.G., and David, C.P.C.: National-scale geodatabase of catchment characteristics in the Philippines for river management applications, PLoS ONE, 18, e0281933, https://doi.org/10.1371/journal.pone.0281933, 2023.
 - Cabrera, J.S. and Lee, H.S.: Flood risk assessment for Davao Oriental in the Philippines using geographic information system-based multi-criteria analysis and the maximum entropy model, J. Flood Risk Mgmt., e12607, 10.1111/jfr3.12607, 2020.
- 625 Coronas, J. The climate and weather of the Philippines, 1903-1918. vol. 25. Bureau of Printing, 1920.
 - Cunnane, C. Unbiased plotting positions a review, J. Hydrology, 37, 205-22, https://doi.org/10.1016/0022-1694(78)90017-3, 1978.
 - Dalrymple, T.: Flood frequency analyses, United States Geological Survey Water Supply Paper, 1543A, 11-51, 1960.
- Fischer, S. and Schumann, A.H.: Handling the stochastic uncertainty of flood statistics in regionalization approaches, Hyd. Sciences J., 10.1080/02626667.2022.2091410, 2022.
 - François, B., Schlef, K.E., Wi, S. and Brown, C.M.: Design considerations for riverine floods in a changing climate A review. J. Hydrology., 574, 557-73, https://doi.org/10.1016/j.jhydrol.2019.04.068, 2019.
- Franco-Villoria, M., Scott, E.M. and Hoey, T.B.: Spatiotemporal modeling of hydrological return levels: a quantile regression approach. Envirometrics, 30, e2522, doi.org/10.1002/env.2522, 2018.
 - Grafil, L. and Castro, O. 2014. Acquisition of IfSAR for the production of nationwide DEM and ORI for the Philippines under the unified mapping project. Infomapper. 21, 12-13 and 40-43.
- Griffiths, G.A., Singh, S.K., and McKerchar, A.I.: Flood frequency estimation in New Zealand using a region of influence approach and statistical depth functions, J. Hydrology., 589, 125187, 10.1016/j.jhydrol.2020.125187, 2020.
 - Ibarra, D. E., David, C. P. C., and Tolentino, P. L. M.: Technical note: Evaluation and bias correction of an observation-based global runoff dataset using streamflow observations from small tropical catchments in the Philippines, Hydrol. Earth Syst. Sci., 25, 2805–2820, https://doi.org/10.5194/hess-25-2805-2021, 2021.
- Irrigation Division: Surface Water Supply of the Philippine Islands 1908-1922. Volumes I V, Bureau of Public Works, Manila, 1923-24.
 - Haberlandt, U. and Radtke, I., Hydrological model calibration for derived flood frequency analysis using stochastic rainfall and probability distributions of peak flows, Hydrology and Earth System Science, 18,353–365, doi:10.5194/hess-18-353-2014, 2014.
- Hosking, J.R.M.: L-moments: analysis and estimation of distributions using linear combinations of order statistics, J. Royal Stat. Soc., Ser. B, 52, 105 124, https://doi.org/10.1111/j.2517-6161.1990.tb01775.x, 1990.
 - Hosking, J.R.M. and Wallis, J.R., Regional frequency analysis: an approach based on L-moments, Cambridge, Cambridge University Press, 1997.
- Kalai, C., Mondal, A., Griffin, A. and Stewart, E.: Comparison of Nonstationary Regional Flood Frequency Analysis Techniques Based on the Index-Flood Approach, J. Hydrol. Eng., 10.1061/(ASCE)HE.1943-5584.0001939, 2020.
 - Kjeldsen, T.R.: How reliable are design flood estimates in the UK? J. Flood Risk Mgmt., 8, 237-246, https://doi.org/10.1111/jfr3.12090, 2013.
 - Kjeldsen, T.R. and Jones, D.A.: Prediction uncertainty in a median-based index flood method using L moments, Water Resour. Res., 42, W07414, https://doi.org/10.1029/2005WR004069, 2006.

- Kjeldsen, T.R., Jones, D.A. and Bayliss, A.C.: Improving the FEH statistical procedures for flood frequency estimation, Environment Agency Science Report SC050050, 2008.
 - Kundzewicz, Z.W., Krysanovab, V., Dankersc, R., Hirabayashid, Y., Kanaee, S., Hattermannb, F.F., Huang, S., Milly, P.C.D., Stoffel, M., Driessenk, P.P.J., Matczaka, P., Quevauvillermand, P. and Schellnhuber, H.-J., Differences in flood hazard projections in Europe—their causes and consequences for decision making. Hydrol. Sci. J., 62, 1–14, https://doi.org/10.1080/02626667.2016.1241398, 2017.
 - Liongson, L.Q.: Regional flood frequency analysis for Philippine rivers. 2nd APHW Conference, Asia Pacific Association of Hydrology and Water Resources, Singapore 2004.
 - Loebis, J.: Frequency analysis models for long hydrological time series in Southeast Asia and the Pacific region, Proceedings of the Fourth International FRIEND Conference, IAHS Publication No. 274, 213-9, 2022.
- Lyubchich V., Newlands N.K., Ghahari A., Mahdi T. and Gel, Y.R. Insurance risk assessment in the face of climate change: Integrating data science and statistics. WIREs Comput Stat., 11,e1462, https://doi.org/10.1002/wics.1462, 2019.
 - Macdonald, N., Kjeldsen, T.R., Prosdocimi, I. and Sangster, H.: Reassessing flood frequency for the Sussex Ouse, Lewes: the inclusion of historical flood information since AD 1650, Nat. Hazards Earth Syst. Sci., 14, 2817-28, doi:10.5194/nhess-14-2817-2014, 2014.
 - Mamun, A.A., Hashim, A. and Amir, Z.: Regional statistical models for the estimation of flood peak values at ungauged catchments: Peninsular Malaysia, J. Hydraul. Eng., 17, 547-553, https://doi.org/10.1061/(ASCE)HE.1943-5584.0000464, 2011.
- Meigh, J.: Regional flood estimation methods for developing countries. Institute of Hydrology / Overseas Development Administration, Report 95/1, 1995.
 - Meigh, J.R., Farquharson, F.A.K., and Sutcliffe, J.V.: A worldwide comparison of regional flood estimation methods and climate. Hydrol. Sci. Journal, 42, 225-244, 1997.
 - Merz, R. and Blöschl, G.: Flood frequency hydrology: 1. Temporal, spatial, and causal expansion of information, Water Resources Research, 44, W08432, W08432, doi:10.1029/2007WR006744, 2008.
- Muhammad, M. and Lu, A.: Estimating the UK index flood: an improved spatial flooding analysis, Environ. Model. & Assess, 25, 731-748, https://doi.org/10.1007/s10666-020-09713-x, 2020.
 - Nippon Koei, The feasibility study of the flood control project for the Lower Cagayan River in the Republic of the Philippines, 4 Volumes, Japan International Cooperation Agency and Department of Public Works and Highways, the Republic of the Philippines, https://openjicareport.jica.go.jp/pdf/11871175.pdf, 2002.
- Parasiewicz P., King E.L., Webb J.A., Piniewski, M., Comoglio, C., Wolter, C., Buijse, A.D., Bjerklie, D., Vezza, P., Melcher, A., and Suska, S. The role of floods and droughts on riverine ecosystems under a changing climate. Fish Manag. Ecol. 26, 461–473. https://doi.org/10.1111/fme.12388, 2019.
 - R Core Team: R: a language and environment for statistical computing, R Foundation for Statistical Computing, Vienna, Austria. https://www.r-project.org/, 2021.
- Reinders, J.B. and Muñoz, S.E.: Improvements to flood frequency analysis on alluvial rivers using paleoflood data, Water Resources Research, 57, e2020WR028631. https://doi.org/10.1029/2020WR028631, 2021.
 - Rigon, R. Rodriguez-Iturbe, I., Maritan, A., Giacometti, A., Tarboton, D.G. and Rinaldo, A.: On Hack's Law. Water Resources Research, 32, 3367-74, https://doi.org/10.1029/96WR02397, 1996.
- Slater, L.J., Singer, M.B. and Kirchner, J.W.: Hydrologic versus geomorphic drivers of trends in flood hazard. Geophysical Research Letters, 42, 1-7, http://doi.org/10.1002/2014GL062482, 2015.
 - Stedinger, J.R., Vogel, R.M. and Foufoula-Georgiou, E., Frequency analysis of extreme events, Chapter 18 in Maidment, D. (ed) Handbook of Hydrology, McGraw-Hill, New York, 1993.

Stedinger, J.R. and Lu, L.-H.: Appraisal of regional and index flood quantile estimators. Stochastic Hydrology and Hydraulics. 9, 49-75, 1995.

Tolentino, P.L.M., Poortinga, A., Kanamaru, H., Keesstra, S., Maroulis, J., David, C.P.C. and Ritsema, C.J., Projected impact of climate change on hydrological regimes in the Philippines, PLOS One, 11, e0163941, doi:10.1371/journal.pone.0163941, 2016.

Yatagai, A., Kamiguchi, K., Arakawa, O., Hamada, A., Yasutomi, N. and Kitoh, A. Constructing a long-term daily gridded precipitation dataset for Asia based on a dense network of rain gauges. Bulletin of the American Meteorological Society. 93(9), 1401-1415, https://doi.org/10.1175/BAMS-D-11-00122.1, 2012.

Zhao, G., Bates, P., Neal, J. and Pang, B.: Design flood estimation for global river networks based on machine learning models, Hydrology and Earth System Sciences, 25, 5981-99, https://doi.org/10.5194/hess-25-5981-2021, 2021.

Ziegler A.D., Lim H.S., Wasson, R.J. and Williamson, F.C.: Flood mortality in SE Asia: Can palaeo-historical information help save lives? Hydrological Processes, e13989.https://doi.org/10.1002/hyp.139898of8, 2020.

720

710

725

730

SUPPLEMENTARY INFORMATION

Table S1. Q_2 equations for different groups of regions. Meigh (1995) did not include regions 13 or CAR, so the total number of sites in the three groups is 431.

Group	Regions in group	Number of sites	Equation	\mathbb{R}^2	se
Growth cu	irve				
A	1,13,CAR	65	$Q_2 = 0.0675(A.RMED)^{0.765}$	0.74	0.287
В	2,3,4A,6,11,12	241	$Q_2 = 0.0218(A.RMED)^{0.836}$	0.68	0.387
C	4B,5,7,10	126	$Q_2 = 0.139(A.RMED)^{0.662}$	0.45	0.443
D	8,9	34	$Q_2 = 0.145(A.RMED)^{0.685}$	0.75	0.203
K-means o	clustering of regional regr	ession equation	ns		
E	1,6,7,8,11	142	$Q_2 = 0.0222(A.RMED)^{0.851}$	0.73	0.336
F	2,3,4A,CAR	167	$Q_2 = 0.0172(A.RMED)^{0.864}$	0.71	0.391
G	4B,9,10,12,13	103	$Q_2 = 0.148(A.RMED)^{0.659}$	0.59	0.376
Н	5	54	$Q_2 = 0.693(A.RMED)^{0.500}$	0.30	0.457
Meigh (19	95) contiguous regional g	roups	, , ,		
Ι	1,2	86	$Q_2 = 0.0513(A.RMED)^{0.779}$	0.63	0.369
J	3,4A,4B,5,6,7,8	264	$Q_2 = 0.0583(A.RMED)^{0.759}$	0.61	0.408
K	9,10,11,12	817	$Q_2 = 0.0723(A.RMED)^{0.696}$	0.57	0.342

Table S2. Q_{100} equations for different groups of regions. Meigh (1995) did not include regions 13 or CAR, so the total number of sites in the three groups is 431.

Group	Regions in group	Number of sites	Equation	\mathbb{R}^2	se
Growth cur	rve				
A	1,13,CAR	65	$Q_{100} = 0.366(A.RMED)^{0.750}$	0.77	0.255
В	2,3,4A,6,11,12	241	$Q_{100} = 0.248(A.RMED)^{0.751}$	0.59	0.425
C	4B,5,7,10	126	$Q_{100} = 6.026(A.RMED)^{0.447}$	0.27	0.447
D	8,9	34	$Q_{100} = 2.023(A.RMED)^{0.537}$	0.60	0.228
K-means cl	lustering of regional regre	ession equation			
E	1,6,7,8,11	142	$Q_{100} = 0.244(A.RMED)^{0.772}$	0.72	0.312
F	2,3,4A,CAR	167	$Q_{100} = 0.184(A.RMED)^{0.787}$	0.63	0.421
G	4B,9,10,12,13	103	$Q_{100} = 4.198(A.RMED)^{0.477}$	0.41	0.393
Н	5	54	$Q_{100} = 24.95(A.RMED)^{0.298}$	0.09	0.520
Meigh (199	95) contiguous regional g	roups			
I	1,2	86	$Q_{100} = 0.317(A.RMED)^{0.756}$	0.58	0.399
J	3,4A,4B,5,6,7,8	264	$Q_{100} = 1.122(A.RMED)^{0.621}$	0.48	0.427
K	9,10,11,12	81	$Q_{100} = 4.111(A.RMED)^{0.446}$	0.33	0.359

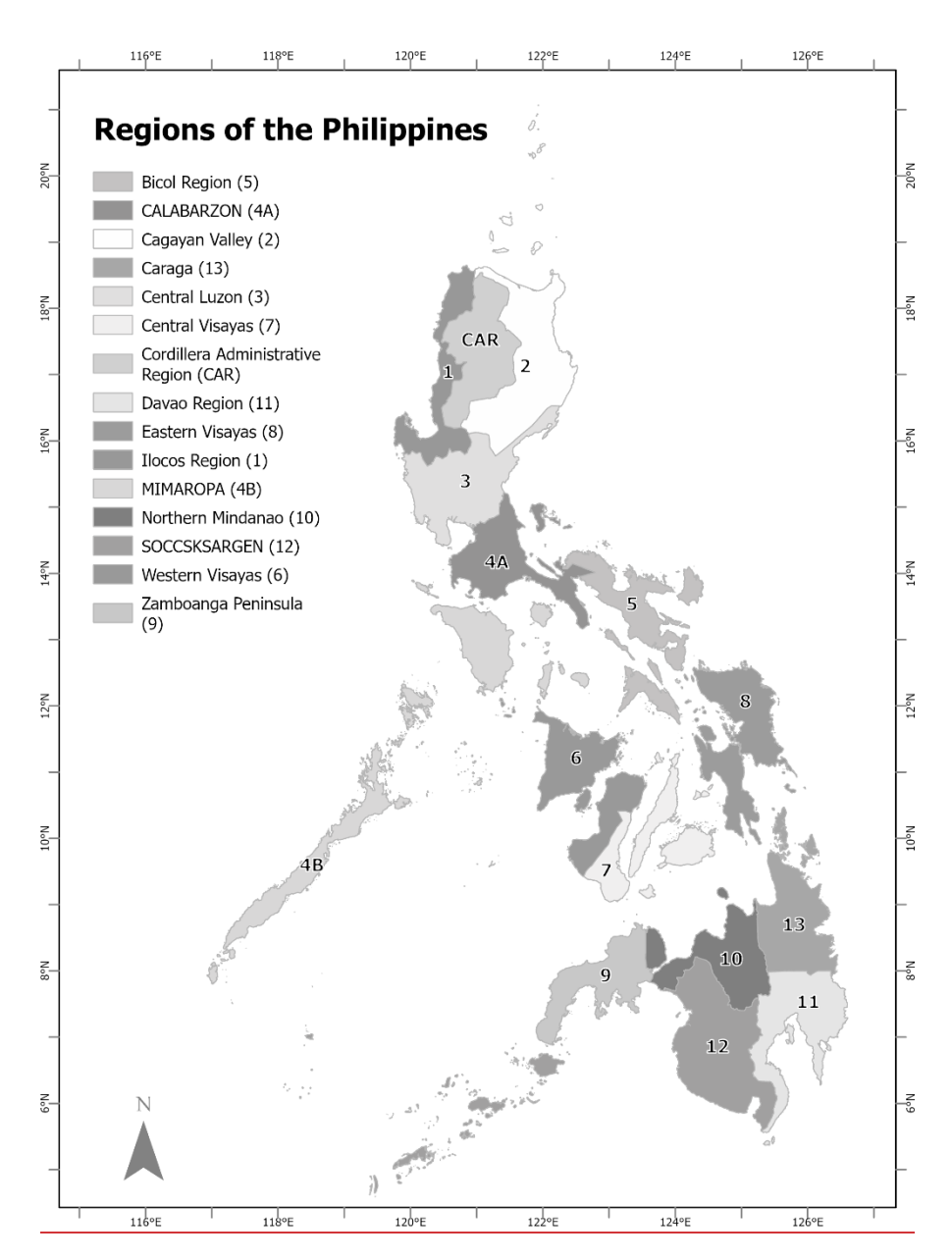


Figure S1. Administrative regions of the Philippines.

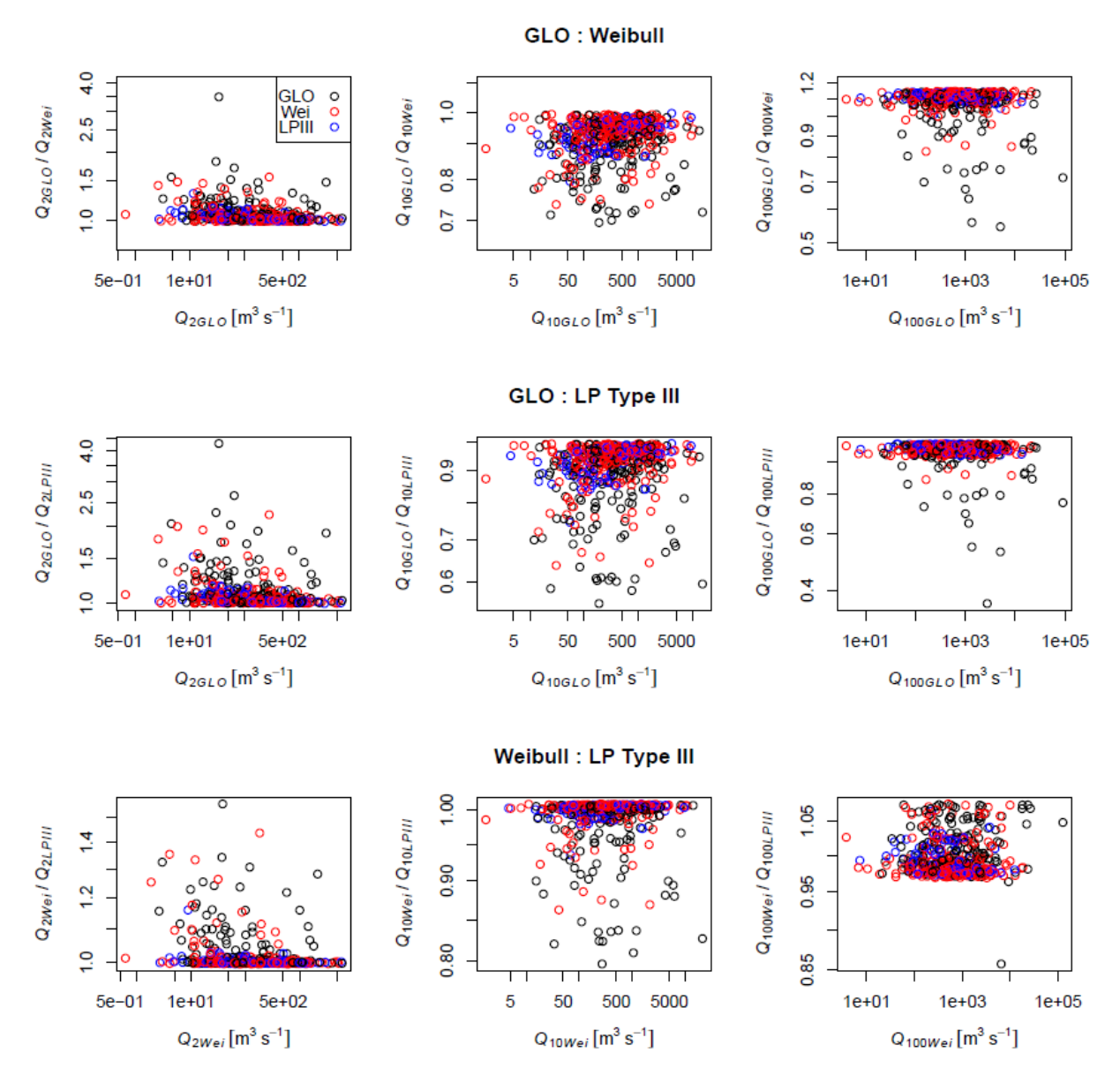


Figure S12. Comparison between flood estimates for 2, 10 and 100 year return periods determined from the three curve fitting methods. GLO = Generalised Logistic Distribution; Wei = Weibull distribution; LPIII = Log-Pearson Type III. x-axes are flood estimates from the GLO (upper two rows) and Weibull distributions, and y-axes are ratios between the estimates obtained from two of the methods, as indicated for each row. Data are colour-coded according to the best-fit curve for each site.

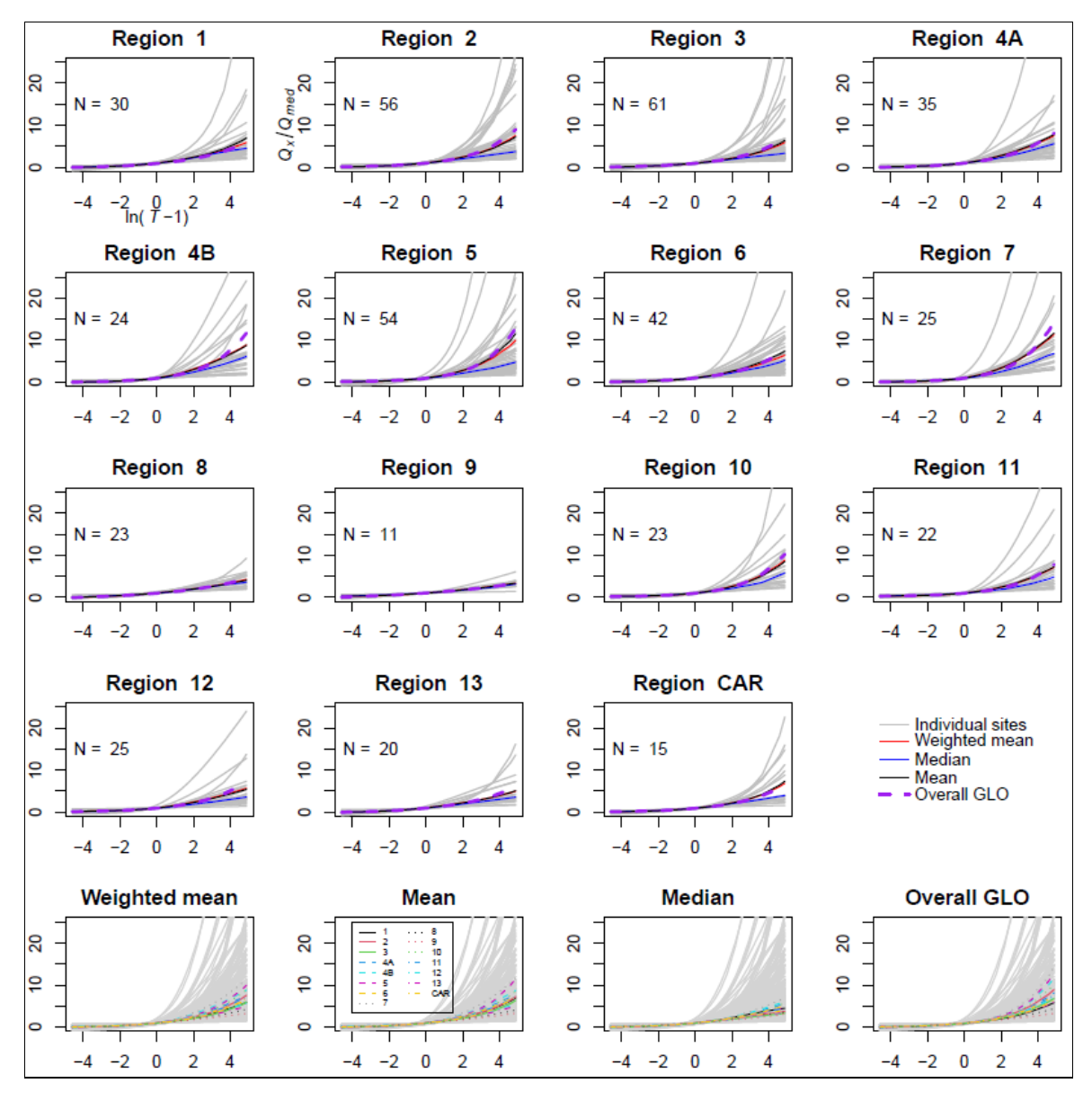


Figure S32. Growth curves for all sites in each region of the Philippines (grey lines) with four methods for calculating a single growth curve for each region. Black line – mean of growth curves for all sites; red line – mean of growth curves for all sites weighted by length of record; blue line – median of growth curves for all sites; and, purple dashed line – GLO curve fitted amalgamated data from all sites within the region. Bottom row shows comparison between the four methods of calculating single growth curves for each region.

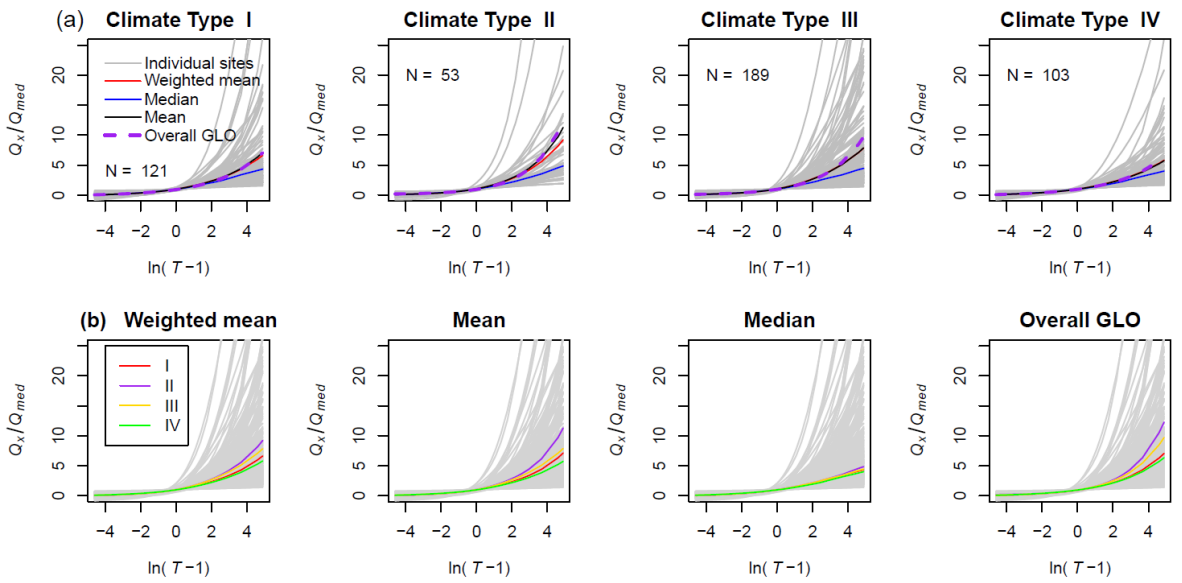


Figure S34. (a) Growth curves for all sites in each climate type of the Philippines (grey lines) with four methods for calculating a single growth curve for each climate type (N is the number of sites of each climate type). Black line – mean of growth curves for all sites; red line – mean of growth curves for all sites weighted by length of record; blue line – median of growth curves for all sites; and, purple dashed line – GLO curve fitted amalgamated data from all sites within each climate type. (b) Comparison between the four methods of calculating single growth curves for catchments within each climate type. Grey lines are growth curves for all individual sites.

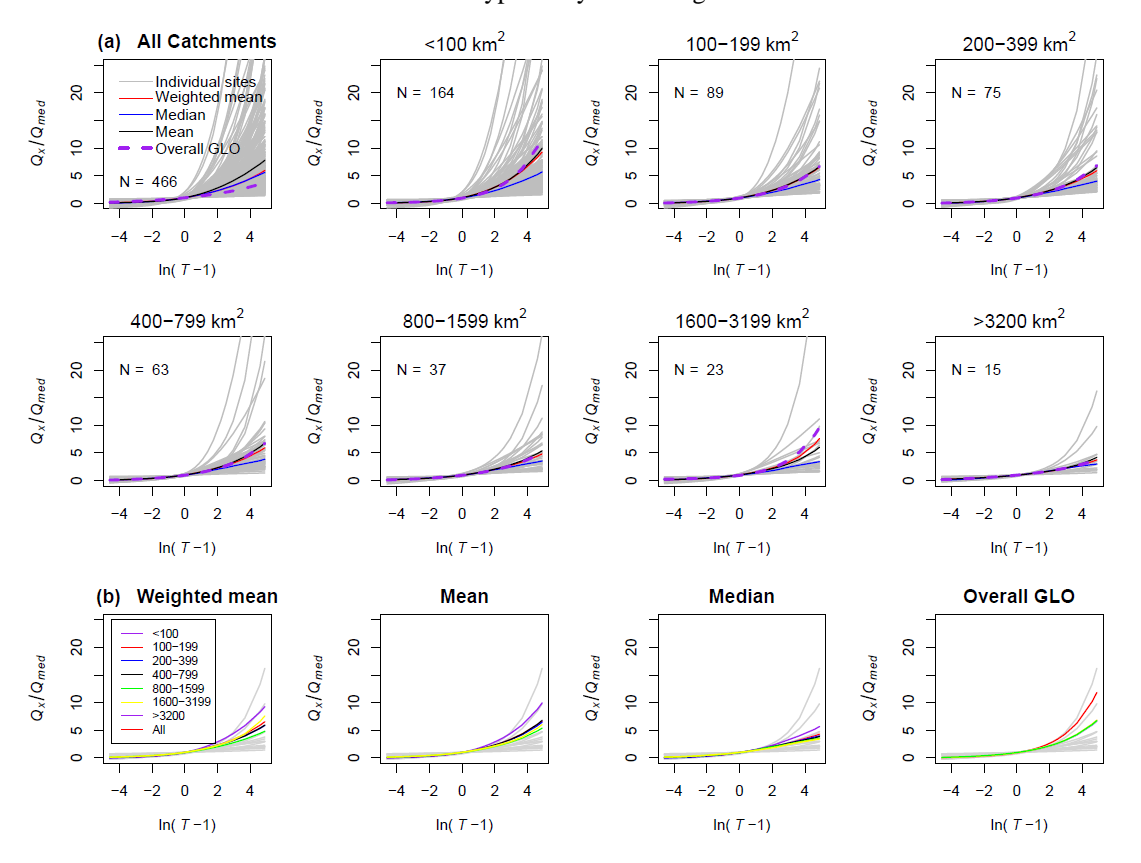


Figure S45. (a) Growth curves for all catchments within catchment area bins indicated (grey lines) with four methods for calculating a single growth curve for each region. Black line – mean of growth curves for all sites; red line – mean of growth curves for all sites weighted by length of record; blue line – median of growth curves for all sites; and, purple dashed line – GLO curve fitted amalgamated data from all sites within each catchment area bin. (b) Comparison between the four methods of calculating single growth curves for within each catchment area bin.

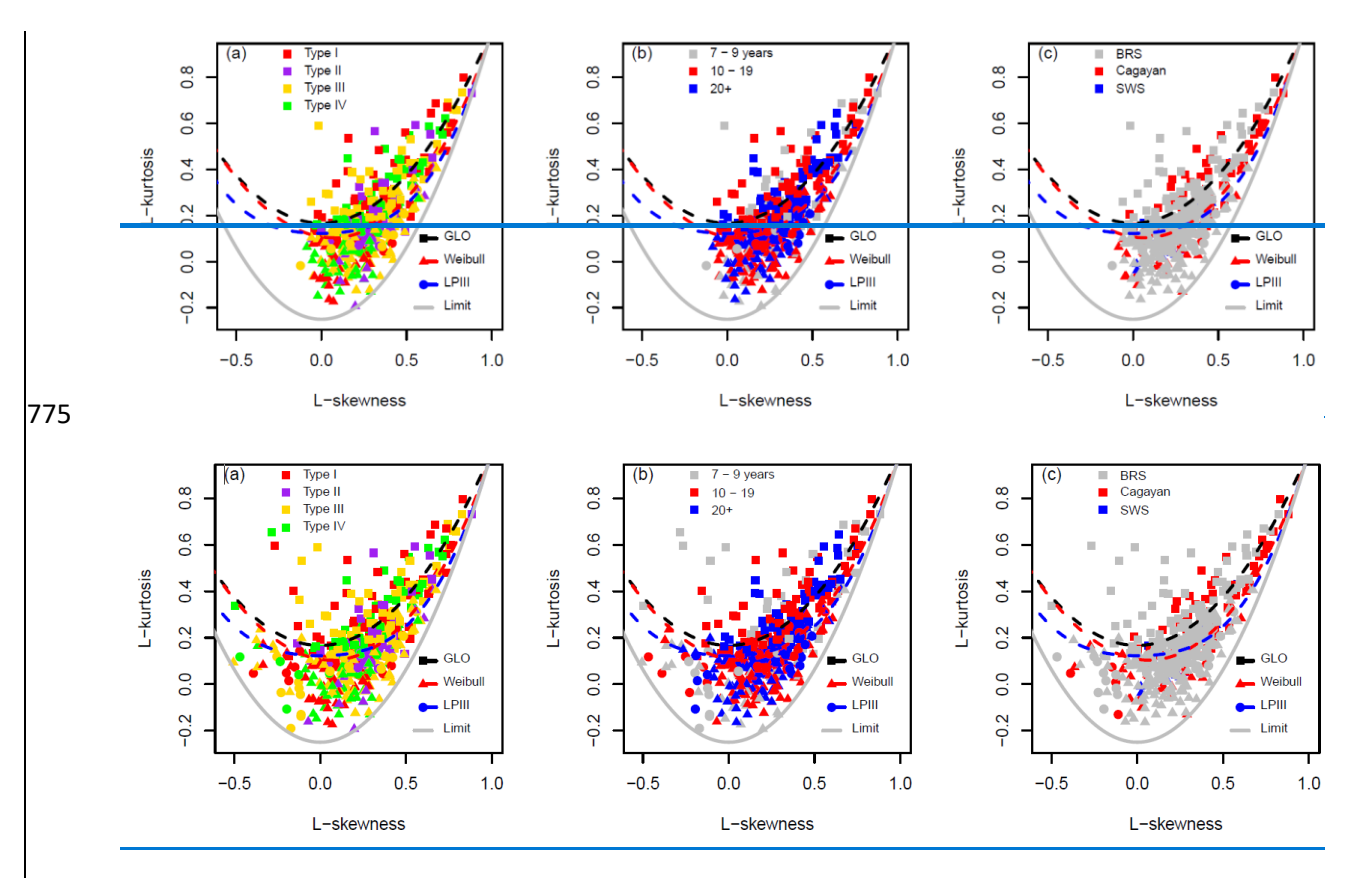
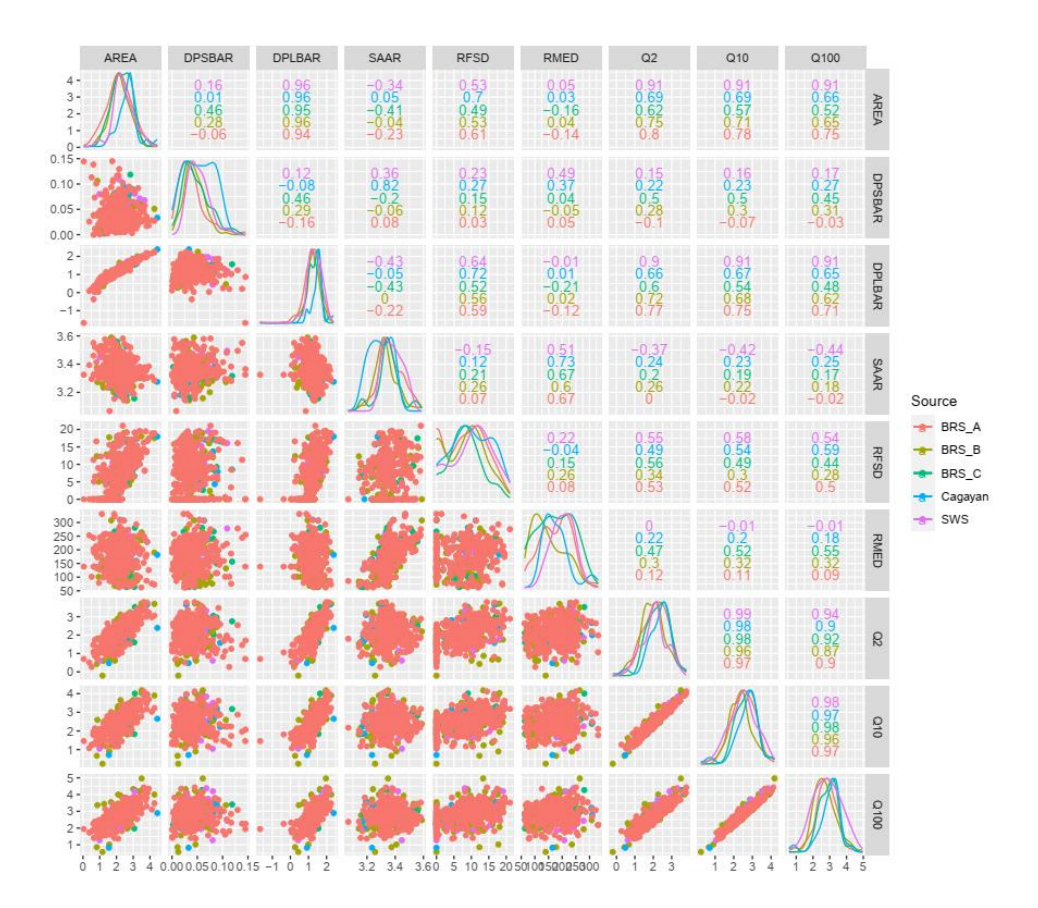


Figure S56. Relationships between L-skewness and L-kurtosis compared with theoretical curves (Hosking and Wallis, 1997). Data classified by: (a) climate zone; (b) length of data record; and, (c) data source. In all cases there is overlap between the best-fit curve type and the classification variable with no obvious clustering of catchments according to climate type, record length or data source. Data points are coloured according to the classification variable, with symbol shape indicating the best-fit curve.



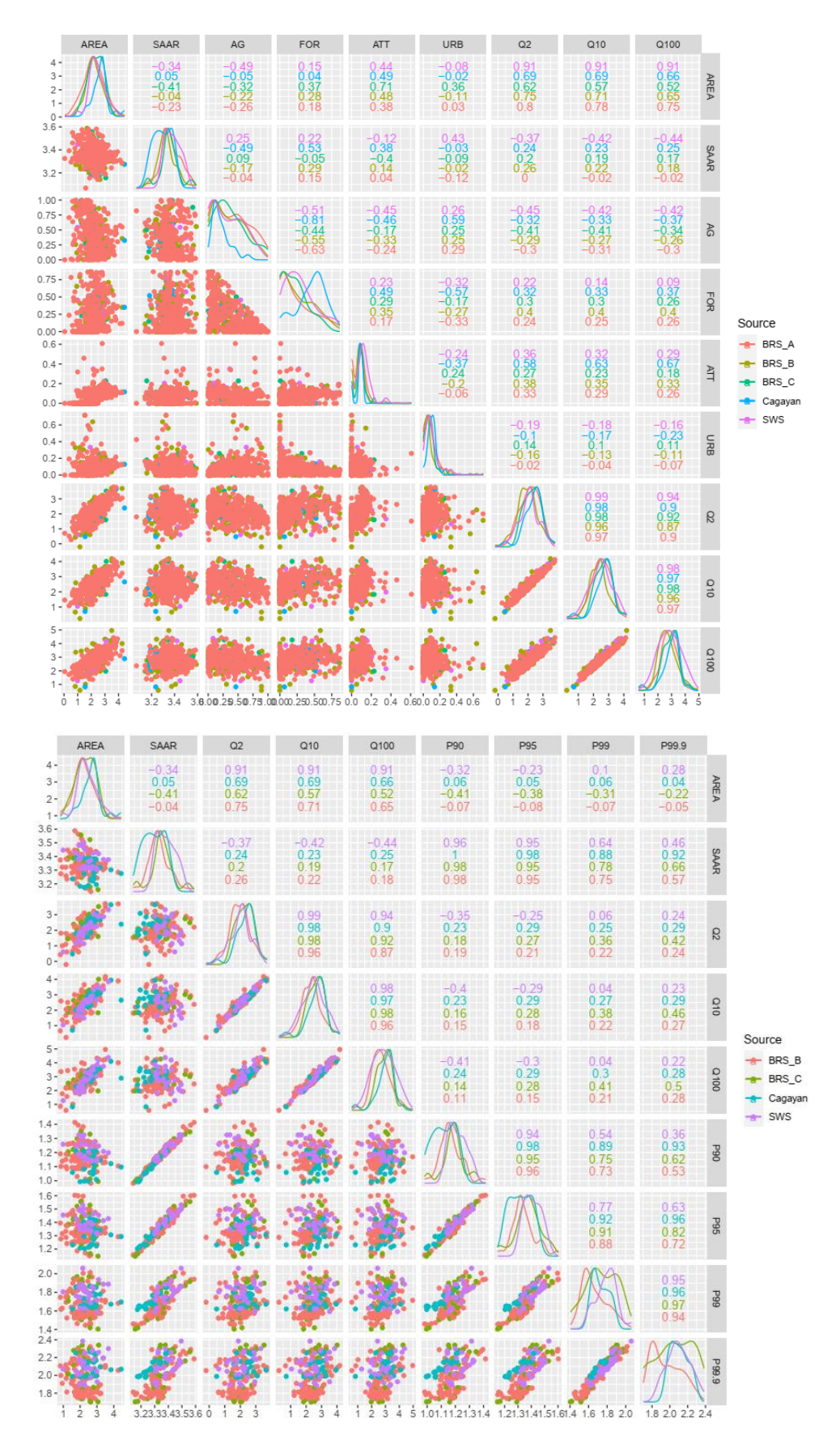


Figure S67. Cross-correlations between all variables used in the analysis. Note that several variables have been transformed prior to plotting, either Log10 (*AREA*, *DPLBAR*, *SAAR*, Q_{MED} , Q_2 , Q_{10} , Q_{100}) or square root (*ATT*, *RFSD*, *URB*). See Table 4 for details. Points are colour coded by data source. Plots on the diagonal are probability

795

density functions of the variables. Numbers on the upper right of each figure are correlation coefficients, also coloured by data source.

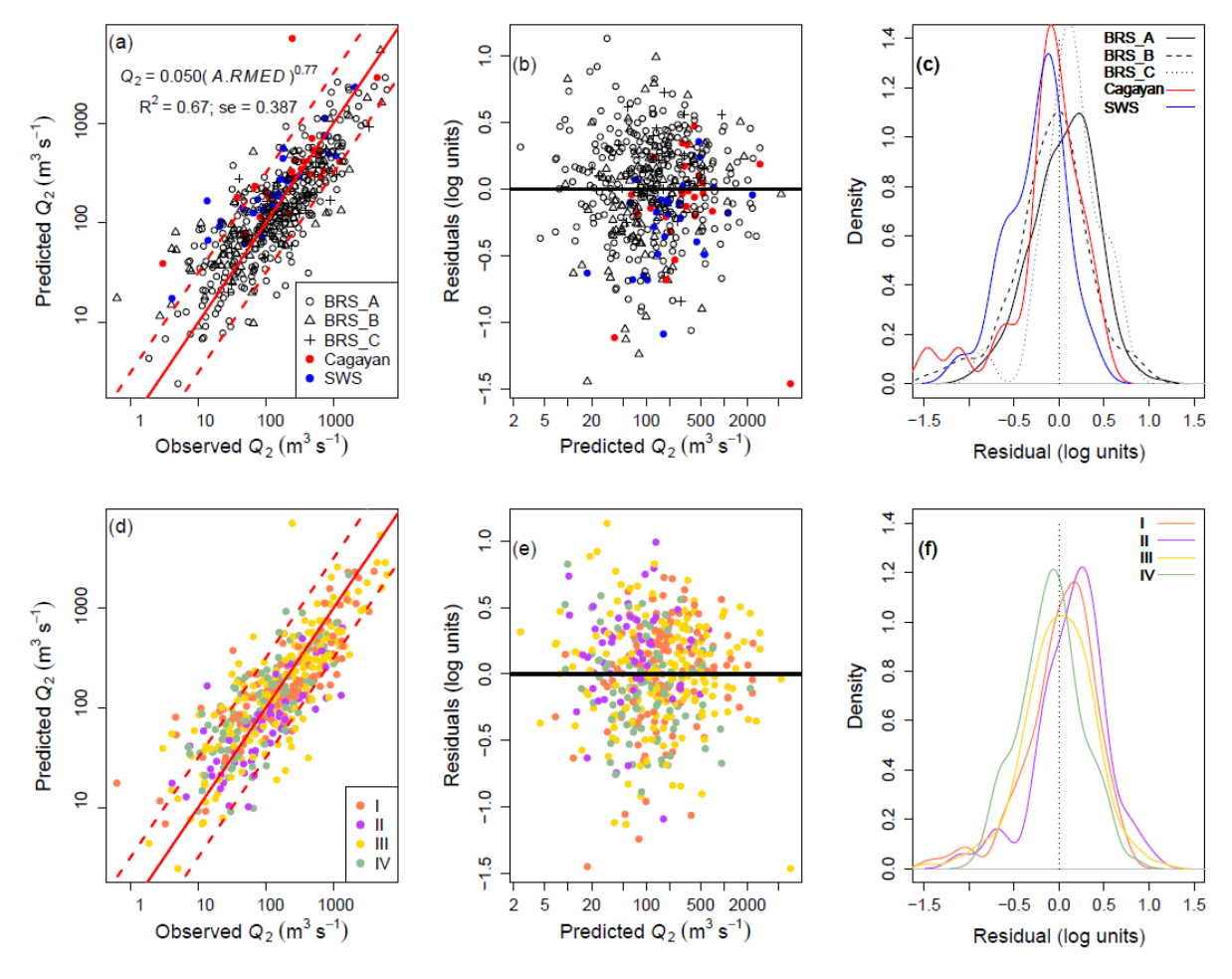


Figure S78. Observed values, prediction and residuals for Q_2 as a function of catchment area (A) multiplied by median daily maximum rainfall (*RMED*). (a)-(c) stratified by data source, (d)-(f) by climate type. (a),(d) are predicted vs. observed values, with 1:1 (solid), 1:2 and 2:1 (dashed) lines shown. Residuals (b) and (e) are normally distributed and show no systematic variation with predicted Q_2 . Density plots of residuals (c), (f) confirm the absence of systematic variation with data source and climate type.

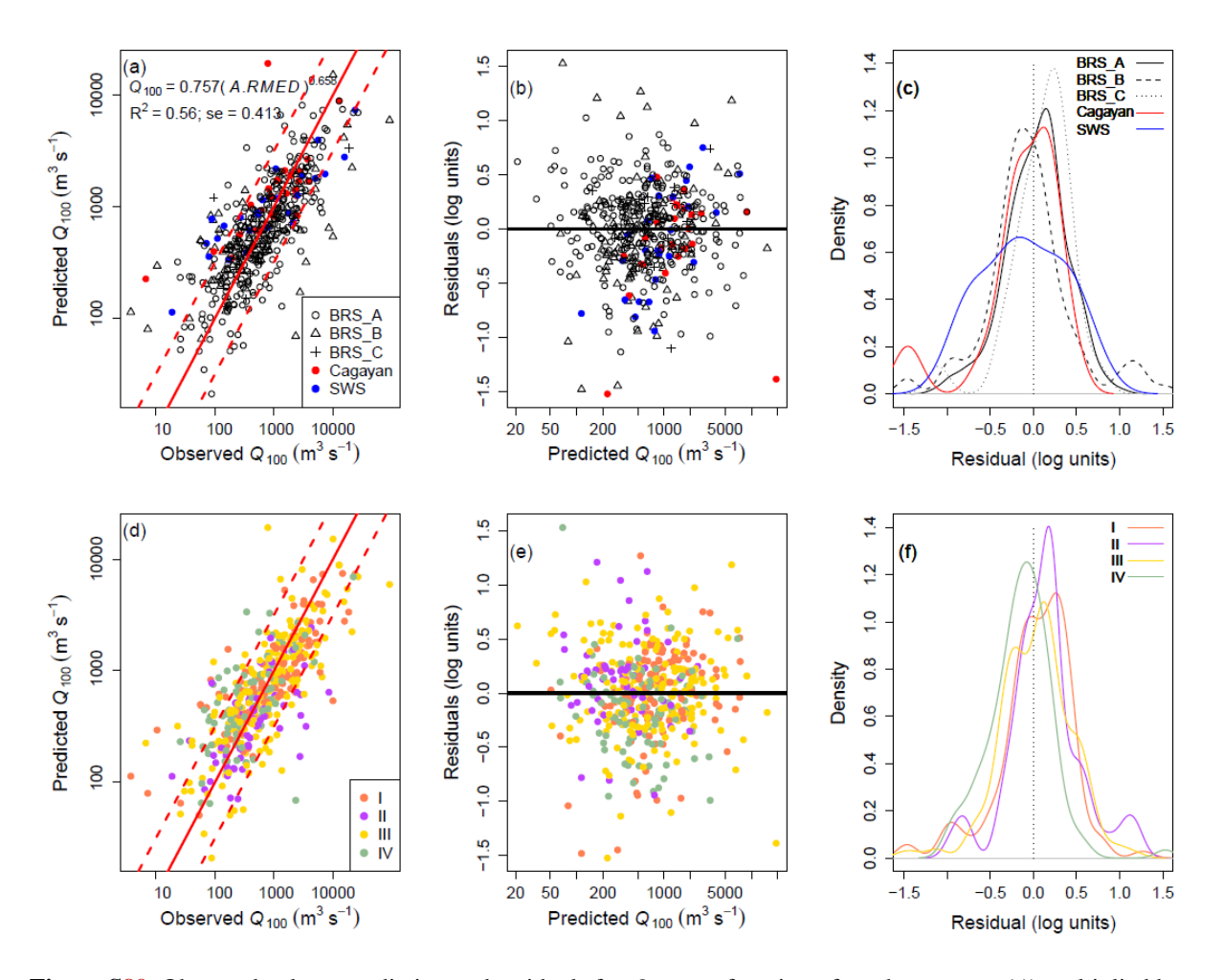


Figure S89. Observed values, prediction and residuals for Q_{100} as a function of catchment area (A) multiplied by median daily maximum rainfall (*RMED*). (a)-(c) stratified by data source, (d)-(f) by climate type. (a),(d) are predicted vs. observed values, with 1:1 (solid), 1:2 and 2:1 (dashed) lines shown. Residuals (b) and (e) are normally distributed and show no systematic variation with predicted Q_{100} . Density plots of residuals (c), (f) confirm the absence of systematic variation with data source and climate type.

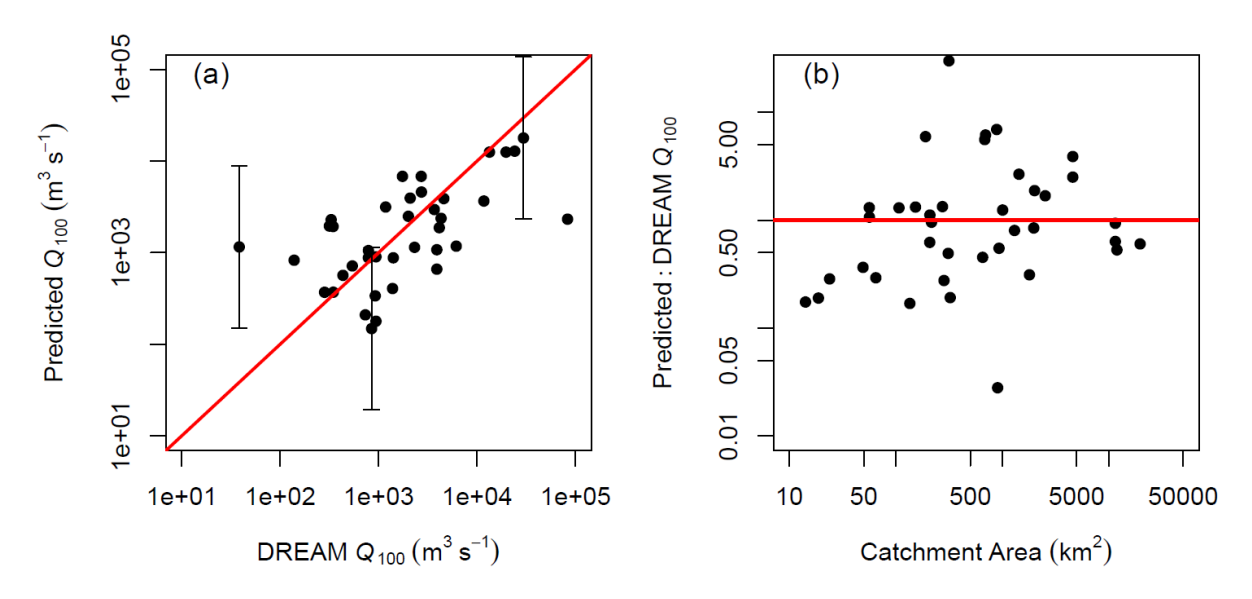


Figure S109. (a) Comparison between Q_{100} estimates based on catchment area (Table 5) and HEC-HMS estimates from the DREAM project. Red line is 1:1 equivalence. (b) Effect of catchment area on the ratio between Q_{100} values from this paper and the DREAM HEC-HMS modelling. Red line shows equal Q_{100} values from both

methods. DREAM estimates are instantaneous peak flows whereas the estimates herein are daily means. As catchment area increases, equivalence between the two methods would show the Q_{100} ratio increasing towards 1.0 as catchment area increases, with lower values in smaller catchments in which flood peaks are of much less than one day duration. 95% prediction intervals are shown for selected points on (a) to indicate the magnitude of statistical uncertainty in the predictions. These are approximated as ± 2 s.e., where s.e. is the regression standard error given in Table 5.